

Inferring climate sensitivity from volcanic events

G. J. Boer · M. Stowasser · K. Hamilton

Received: 10 May 2006 / Accepted: 6 September 2006 / Published online: 6 December 2006
© Springer-Verlag 2006

Abstract The possibility of estimating the equilibrium climate sensitivity of the earth-system from observations following explosive volcanic eruptions is assessed in the context of a perfect model study. Two modern climate models (the CCCma CGCM3 and the NCAR CCSM2) with different equilibrium climate sensitivities are employed in the investigation. The models are perturbed with the same transient volcano-like forcing and the responses analysed to infer climate sensitivities. For volcano-like forcing the global mean surface temperature responses of the two models are very similar, despite their differing equilibrium climate sensitivities, indicating that climate sensitivity cannot be inferred from the temperature record alone even if the forcing is known. Equilibrium climate sensitivities can be reasonably determined only if both the forcing and the change in heat storage in the system are known very accurately. The geographic patterns of clear-sky atmosphere/surface and cloud feedbacks are similar for both the transient volcano-like and near-equilibrium constant forcing simulations showing that, to a considerable extent, the same feedback processes are invoked, and determine the climate sensitivity, in both cases.

1 Introduction

Climate sensitivity is a measure of the strength of the connection between a perturbation to the earth's radiation balance, due to greenhouse gases, aerosols, or other natural or anthropogenic forcings, and the resulting change in global mean surface temperature. A high value of climate sensitivity means that the climate system responds strongly to a radiative perturbation to produce a comparatively large temperature change (and by inference concomitantly large changes in other climate parameters). A low value of climate sensitivity means the climate system will produce only modest changes in temperature for the same radiative perturbation. The “sensitivity” of the earth's climate system is obviously a critical parameter in the debate over controlling and mitigating global warming. Unfortunately, the earth's climate sensitivity is not accurately known.

The *equilibrium* climate sensitivity is defined here as the factor of proportionality \hat{s} in the relationship $\langle T' \rangle = \hat{s} \langle f \rangle$ where $\langle T' \rangle$ is the global mean (indicated by angular brackets) temperature change that is attained after the climate system has reached a new equilibrium under constant forcing with global mean value $\langle f \rangle$. The value of \hat{s} is a comparatively robust feature of a climate model, and presumably of the real system, for different forcing mechanisms. Thus, to first order, the global mean temperature response for a change in CO₂ or for a change in solar input, for instance, depends on the magnitude of the forcing $\langle f \rangle$ and not on the differing patterns of the forcing nor the fact that one depends on forcing in the infrared and the other in the shortwave (IPCC2001, Sect. 6.2). A common alternative definition of climate sensitivity is the equilibrium global

G. J. Boer (✉)
Canadian Centre for Climate Modelling and Analysis,
Environment Canada, University of Victoria,
Victoria, BC, Canada V8W 2Y2
e-mail: George.Boer@ec.gc.ca

M. Stowasser · K. Hamilton
International Pacific Research Centre,
University of Hawaii, Honolulu, HI 96822, USA

mean temperature change $\langle T'_{2x} \rangle$ for the “standard” forcing imposed by a doubling of the CO₂ concentration in the model atmosphere.

The *equilibrium* climate sensitivity is defined in terms of the response of the system to a constant imposed forcing after the climate system has come into a new equilibrium with it. A more general approach (Boer and Yu 2003a), discussed in Sect. 3, defines a climate sensitivity parameter \hat{s} for non-equilibrium conditions. Although \hat{s} is reasonably constant to first order there are indications of changes with forcing level (e.g. the NCAR model for strong forcings as discussed in Boer et al. 2005) and of modest changes as the climate evolves under constant forcing (Boer and Yu 2003b; Senior and Mitchell 2000; Stowasser et al. 2006). In climate change experiments the forcing may either be “stabilized” (i.e. held constant) after an initial period of increase or the forcing may simply be imposed at a constant value. In either case, the time-series of \hat{s} , determined from each year of the simulation, tends fairly quickly toward a value that is reasonably close to the equilibrium value.

There remains considerable uncertainty in our knowledge of the sensitivity of the real climate system. Although the climate sensitivity is generally a robust parameter for a climate model, it may have different values for different models. The range of climate sensitivities determined from sophisticated climate models varies by more than a factor of two (IPCC 2001, Fig. 9.18; IPCC 2004). Ideally, observations of the real system would be used to infer climate sensitivity and there is a long history of efforts to infer its value from past behaviour, including considerations of ice ages, recent climate evolution and the natural experiments provided by volcanoes (e.g. Wigley et al. 2005a, b; IPCC2004, and references therein). These efforts have met with only moderate success, however, because the natural variability of the climate system, the lack of accurate knowledge of the radiative perturbations involved, energy storage in the ocean, and the nature of the response of the climate system all confound the analysis. The result is that a rather broad range of climate sensitivities are “not inconsistent” with the observational evidence.

Observations of climate system behaviour following large explosive volcanic eruptions would appear to offer a reasonable possibility of inferring the earth’s climate sensitivity. After a major eruption the resulting volcanic cloud of sulfuric acid aerosols reflects incoming solar radiation and produces a negative climate forcing of several Wm⁻² which acts to cool the surface. This negative forcing decays away over several years, as the aerosol is removed from the atmosphere, and the

global surface temperature recovers over a somewhat longer period. Since the advent of reasonably widespread instrumental temperature records in the nineteenth century there have been several eruptions strong enough to produce a measurable effect on global surface temperature, the most recent being the eruption of Mt. Pinatubo in 1991 (e.g. Robock and Mao 1995).

The difficulties in inferring climate sensitivities from observations, mentioned earlier, remain however. In addition, the response of the climate system to a short timescale volcano-like perturbation may not be representative of the long timescale response which characterizes the equilibrium climate sensitivity. The lack of, or partial knowledge of, the volcanic radiative forcing will confound the analysis as will the natural variability of the system together with imperfect knowledge of the climatology and global distribution of even such a basic variable as surface temperature.

Here we investigate the potential for inferring climate sensitivity from volcanic events using a “perfect model” approach. We ask if we may successfully infer the climates sensitivities of two sophisticated coupled global climate models from volcano-like perturbation experiments. The two models used are the Canadian Centre for Climate Modelling and Analysis (CCCma) CGCM3 and the National Center for Atmospheric Research (NCAR) CCSM2. We adopt a time-dependent change in solar constant as a proxy for the volcanic perturbation to the radiation balance. This approach provides an unambiguous knowledge of the radiative forcing of the modelled system (Boer et al. 2005). For each model we may diagnose the climate sensitivity for the modelled system based on full knowledge of the radiative fluxes and the temperature behaviour in the volcano-like perturbation experiment and compare it with measures of equilibrium climate sensitivity. We may also attempt to infer the climate sensitivity in an “observational” context, without full knowledge of the system, as might be done for historic or future volcanic events. Finally, the idealized model approach allows us also to analyse and compare feedback processes in the two models under volcano-like time dependent conditions as compared to near-equilibrium constant forcing conditions, following the approach used in Boer and Yu (2003a) and Stowasser et al. (2006).

The paper is organized as follows. In Sect. 2 the two GCMs employed are briefly described and the design of the volcano-like perturbation experiment explained. The diagnostic approach characterizing climate feedbacks and climate sensitivity, which follows from the equations for the energy balance of the climate system, is described in Sect. 3. The surface temperature

responses to volcano-like forcing in the two models are presented and compared in Sects. 4.1–4.3 and Sect. 4.4 considers how well the equilibrium climate sensitivity can be determined if only the surface temperature evolution following an eruption is known. Sections 4.4 and 4.5 consider the diagnosing of the climate sensitivity in cases where independent knowledge of changes in system heat storage is available, and considers how estimates of the climate sensitivity will be affected by inaccuracies in observations of heat storage and surface temperature. Section 5 considers the geographical structures of the climate feedback components in the transient volcano-like perturbation experiments and compares them with the same quantities determined from near equilibrium experiments with constant forcing. Conclusions are presented in Sect. 6.

2 Models and experiments

Two state-of-the-art coupled ocean-atmosphere global climate models are used in this study namely version 2.0.1 of the NCAR Community Climate System Model (CCSM2) and version 3 of the CCCma Coupled Global Climate Model (CGCM3). The NCAR model is described in Kiehl and Gent (2004) and the simulations reported here were performed at IPRC at an atmospheric resolution of T32L26 and an ocean resolution of about 3°. The CCCma model is an outgrowth of CGCM2 (Flato and Boer 2001) incorporating a new version of the atmospheric component as discussed in Scinocca and McFarlane (2004). Simulations are performed at T47L32 dynamical resolution with physics calculations done on the 96×48 linear grid. The ocean model horizontal resolution is twice that of the atmospheric model. The version of the NCAR model used in these experiments is the same as that used in the experiments described in Stowasser et al. (2006) while a slightly updated version of the CCCma model, ported to parallel processing environment, is used here.

As well as integrations with the full coupled atmosphere–ocean models, results are also obtained using a version of the CCCma model with the identical atmospheric component but with the full ocean component replaced by a 50 m deep “mixed layer” or “slab” ocean component in which prescribed ocean energy transports, including heat exchange with the deep ocean, do not change with climate change.

2.1 Volcano-like forcing

The experiments performed consist of imposing volcano-like radiative perturbations on the coupled

models by varying the solar constant. The top of atmosphere (TOA) net downward solar flux may be expressed as $S = (1 - \alpha)(1 + a)\Sigma$ where α is the planetary albedo and Σ the incident solar flux scaled by the fraction $(1 + a)$. For the unperturbed control simulation, $a = 0$, and the TOA solar flux is $S_0 = (1 - \alpha_0)\Sigma$. For radiative perturbations imposed by a time-dependent change in the solar constant $a(t) \neq 0$ the instantaneous radiative forcing is $f(t) \approx a(t)S_0$ to good approximation. Boer et al. (2005) point out that the stratospheric effects are small and Stowasser et al. (2006) show that this forcing in the two models is very nearly identical (to within 1%). For $a = 0.025$, that is for a constant increase in solar constant of 2.5%, the resulting forcing is $f \approx 6 \text{ Wm}^{-2}$, which is comparable to the expected forcing due to increasing GHGs in the twenty-first century.

For the volcano-like experiments we take $a(t) = \left(\frac{f_{\max}}{\langle S_0 \rangle}\right) \left(\frac{t}{\tau}\right) e^{1-(t/\tau)}$, where f_{\max} is the maximum of the forcing, and τ is a forcing timescale. The volcano-like forcing becomes

$$f = aS_0 = S_0 \left(\frac{f_{\max}}{\langle S_0 \rangle}\right) \left(\frac{t}{\tau}\right) e^{1-(t/\tau)} \quad (1)$$

which follows the form adopted by Douglass and Knox (2005a) for the Pinatubo eruption. In our case we choose a value of $\tau = 8$ months which provides a realistic time evolution of volcano-like forcing as indicated in Fig. 1 where a function of this form is fit to the visible optical depth results of Ammann et al. (2003). In this range of aerosol optical depth the shortwave aerosol radiative forcing is nearly linearly proportional to the visible optical depth (Zhang et al. 2005). We choose

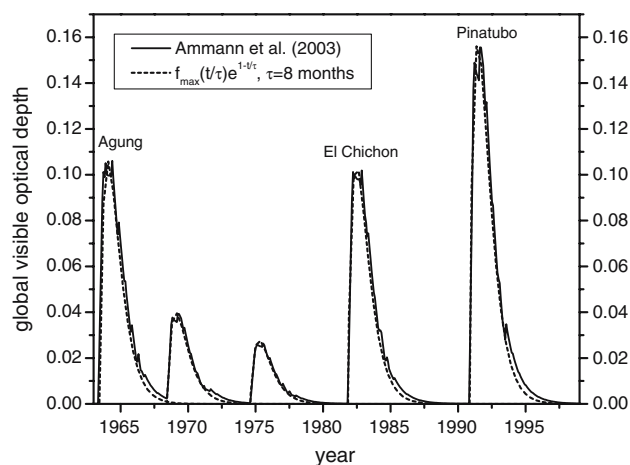


Fig. 1 Globally averaged visible optical depths from the volcanic forcing data set of Ammann et al. (2003) and the fitted function $f_{\max}(t/\tau)e^{1-t/\tau}$ for $\tau = 8$ months

$f_{\max} = 6 \text{ W m}^{-2}$ which may be compared to estimates of the maximum forcing (shortwave plus longwave) for the Pinatubo volcanic episode which range from 3 to 4.5 W m^{-2} (Hansen et al. 1992, 2002). This forcing is chosen both to enhance signal to noise in the analysis and to relate the volcano experiment directly to the 2.5% solar constant increase experiments with the models.

The radiative perturbation employed in these experiments is an idealization of the effects of a real volcanic eruption. Here, the radiative perturbation is in the solar component, mimicking the reflection of solar radiation by the volcanic aerosol. The forcing does not include the absorption of terrestrial radiation and the heating of the stratosphere due to the aerosol. It also takes a few months for the aerosols from low- and mid-latitude eruptions to spread reasonably uniformly over the globe (aerosol clouds produced by high latitude eruptions may stay rather confined to high latitudes). Even for eruptions fairly near the equator there can be a range of behavior in the dispersion of the aerosol as exemplified by the aerosol cloud from Mt. Pinatubo (June 1991, 15 N) which spread fairly uniformly into both the Northern and Southern Hemispheres, that from El Chichon (April 1982, 18 N) which initially spread mainly into the Northern Hemisphere, and that from Mt. Agung (March 1963, 8 S) which initially spread mainly into the Southern Hemisphere (e.g. Fig. 3 of Hansen et al. 2002). Even in the cases of El Chichon and Mt. Agung, however, the aerosol has spread globally in about a year. Although some time is required for the aerosol to attain a more or less uniform distribution, atmospheric energy transport helps spread the effect of the forcing around the globe so that the response is not localized to where the forcing occurs (Boer and Yu 2003a). Figure 1 demonstrates that the time evolution of the imposed solar forcing matches that of the observed visible optical depths associated with a typical volcanic event.

2.2 Simulations

The experiment consists of three realizations of an idealized volcano-like climate perturbation with both models. The simulations are of 25 years duration using initial conditions from the respective models' control simulations for 1 January separated by 10 years. A 100 year control simulation provides climatological statistics, including the climatological annual cycle (CAC) of the variables of interest, for each model. Results are also available for 50 year simulations with switch-on solar constant increases of 2.5 and 5% in the manner of Stowasser et al. (2006). Finally, a volcano-

like simulation with the “mixed-layer” ocean version of CGCM3 is performed. In this case there is no change in oceanic horizontal energy transport nor in heat exchange with the deep ocean as climate changes. These different experiments offer the possibility of analyzing and comparing (model-based) climate sensitivity estimates under different forcing conditions with special attention given to volcano-like forcing situations.

3 Climate feedback and climate sensitivity from volcano-like forcing

Monthly mean budget quantities are retained for the simulations and the deviation of a quantity X from its climatological annual cycle (CAC) is obtained as $X' = X - X_0$ where X_0 denotes the CAC obtained from the unforced control simulation.

3.1 The energy budget, forcing and feedback

Following Boer and Yu (2003a) the change in the vertically integrated energy budget of the climate system is written as

$$\begin{aligned} \frac{dh'}{dt} &= A' + R' = A' + (R - R_*) + (R_* - R_0) \\ &= A' + g + f = A' + \Lambda T' + f. \end{aligned} \quad (2)$$

where dh'/dt is the change in the energy stored in the system (primarily in the oceans), A' is the change in the convergence of horizontal energy transports in the atmosphere and ocean and R' is the change in radiative flux into the column.

This radiative flux change is decomposed into response (g) and instantaneous forcing (f) components as indicated in (2) where R_* is the radiative flux that is obtained when the forcing agent is present but the system retains its control run values of other quantities. As discussed in Boer et al. (2005), the shortwave S and longwave L radiative components of the perturbed radiative flux may be written as $R = S - L = (1 - \alpha)(1 + a)\Sigma - L$, where the solar constant increase is indicated by the multiplicative factor $(1 + a)$. For the control run climate $R_0 = S_0 - L_0 = (1 - \alpha_0)\Sigma - L_0$. When the forcing agent is present but without other change, $R_* = (1 - \alpha_0)(1 + a)\Sigma - L_0$ to good approximation in the case of a modification to the solar constant. The forcing and the radiative response are, respectively,

$$f = R_* - R_0 = a(1 - \alpha_0)\Sigma = aS_0 \quad (3)$$

$$g = R - R_* = \alpha'(1 + a)\Sigma - L' \tag{4}$$

The distribution of f for the two models for a 2.5% increase in solar constant ($a = 0.025$) is essentially that of Fig. 1 of Boer et al. (2005) and is not reproduced here. Recall that the incoming radiation Σ varies smoothly with latitude and is constant in longitude while the planetary albedo for the control simulation, α_0 , causes deviations of from this smooth pattern. The forcing is somewhat weaker over the land compared to oceans as a consequence of the larger planetary albedo there. The radiative response may be further decomposed into components associated with different radiative processes as

$$g = (R - R_*) = g_L + g_S = g_A + g_C \\ = g_{LA} + g_{LC} + g_{SA} + g_{SC} \tag{5}$$

where g_L and g_S are the longwave and shortwave components, g_A the clear-sky atmosphere/surface feedback and g_C the cloud feedback components of R and R_* in (4).

The radiative response expressed as a linear function of temperature defines the local feedback parameter Λ from $g = \Lambda(\lambda, \varphi, t)T'$. Normalizing the radiative response by the global mean (indicated by angular brackets) temperature change gives the “local contribution” to the global feedback

$$\Lambda_l = (R - R_*)/\langle T' \rangle = g/\langle T' \rangle \tag{6}$$

where the global feedback parameter $\hat{\Lambda} = \langle \Lambda_l \rangle$ is the global average of the local contribution. The local feedback parameter may also be decomposed into feedback components following (5).

3.2 Global feedback/sensitivity

The globally averaged energy budget of the system from (2) is

$$\langle dh'/dt \rangle = \langle R' \rangle = \langle g \rangle + \langle f \rangle = \hat{\Lambda} \langle T' \rangle + \langle f \rangle \tag{7}$$

since the transport term $\langle A' \rangle = 0$ averages to zero under the global averaging indicated by the angular brackets. The global feedback parameter $\hat{\Lambda} = \langle \Lambda T' \rangle / \langle T' \rangle$ is a temperature weighted average of local values and must be negative if the system is to come to a new equilibrium with an imposed forcing. The connection between the global mean temperature response, forcing, feedback, and sensitivity is

$$\langle T' \rangle = \langle g \rangle / \hat{\Lambda} = \langle dh'/dt - f \rangle / \hat{\Lambda} = \hat{s} \langle f - dh'/dt \rangle \tag{8}$$

where all terms are functions of time. The global feedback and sensitivity parameters are related as $\hat{s} = -1/\hat{\Lambda}$ and may be obtained diagnostically from (7). As the system approaches equilibrium with a given forcing, $\langle dh'/dt \rangle \rightarrow 0$ in (8) and $\langle T' \rangle = \hat{s} \langle f \rangle$ relating the global mean equilibrium temperature response to global mean forcing.

As noted in Sect. 1, experience with climate models indicates that \hat{s} is reasonably constant and independent of the nature of the forcing agent. This justifies the most common measure of climate sensitivity as the equilibrium temperature change due to a doubling of CO₂ in the atmosphere. In that case, $\langle T'_{2x} \rangle = \hat{s} \langle f_{2x} \rangle$ so that, providing the CO₂ forcing is known, \hat{s} and $\langle T'_{2x} \rangle$ contain the same information about how global mean temperature responds to radiative forcing of a given magnitude. There is a considerable difference in the climate sensitivities of models as measured by $\langle T'_{2x} \rangle$, however, which differs by a factor of two or more (IPCC 2001, Fig. 9.18). Moreover, $\langle f_{2x} \rangle$ is not always available and when it is available it may have been calculated using different techniques. Finally, there is an indication that $\langle f_{2x} \rangle$ may differ among current models as a consequence of differences in radiation code implementation (Collins et al. 2006). The approach taken here attempts to circumvent these difficulties by appealing to a particularly simple forcing so that f is well known and by considering explicitly the various terms in the energy budget.

3.3 The global mean surface temperature equation

An equation for the global mean surface temperature follows from (7) provided the storage term can be suitably expressed. In this section we deal with globally averaged quantities but drop the angular brackets for notational convenience. The usual approach (e.g. IPCC 2001; Boer et al. 2005) considers the energy equation for the surface (that is, the mixed layer of the ocean and the surface layer of the land) and expresses the storage term as $dh'/dt = CdT'/dt + F'_0$ where C is the heat capacity of the layer and F'_0 is the perturbation flux of energy out of the layer into the deep ocean. A reasonable assumption is that this flux is proportional to the temperature perturbation $F'_0 \approx \kappa T'$, at least over the comparatively short timescales of a volcano-like event, and this allows the temperature equation to be written as

$$C \frac{dT'}{dt} = \hat{\Lambda} T' + f - F'_0 = (\hat{\Lambda} - \kappa) T' + f = \hat{\Lambda}_* T' + f. \tag{9}$$

where $\hat{\Lambda}_* = \hat{\Lambda} - \kappa = -(1/\hat{s} + \kappa) = -(1 + \hat{s}\kappa)/\hat{s} < 0$ is an “effective” feedback parameter incorporating also the

flux into the deep ocean. The solution to (9) for forcing of the form (1) is

$$T'(t) = \frac{f_{\max}}{C(1-\beta\tau)^2} \left\{ \tau e^{1-\beta t} - (\tau + (1-\beta\tau)t) e^{1-t/\tau} \right\} \quad (10)$$

where $\beta = -\hat{\Lambda}_*/C = -(\hat{\Lambda} - \kappa)/C = (1 + \kappa\hat{s})/\hat{s}C > 0$.

If there is little flux into the deep ocean $\hat{\Lambda} \approx \hat{\Lambda}_*$. Otherwise, $\hat{\Lambda}_* = \hat{\Lambda} - \kappa < \hat{\Lambda}$ and the effective feedback is larger negative than the actual feedback. Fitting (10) to the temperature record gives β and C and hence $\hat{\Lambda}_* = -C\beta$. However $\hat{\Lambda}$ cannot be inferred from $\hat{\Lambda}_*$ unless κ is known or the flux into the deep ocean can be neglected. Neglecting the flux into the deep ocean when it is not small (or setting κ to 0) overestimates the strength of the negative feedback and underestimates the climate sensitivity.

3.4 Climate feedback/sensitivity and volcanoes

We attempt to answer the following questions: what are the models' *equilibrium* climate feedback/sensitivities under known constant forcings from increases of 2.5 and 5% in the solar constant; what are the models' climate feedback/sensitivities inferred from the volcano-like experiments under a range of assumptions about our knowledge of the system; how confident can we be of observationally-based sensitivity inferences based on volcanoes; what local feedback processes dominate the inferred sensitivity for volcano-like forcing, do they differ from the equilibrium case, and how do they compare between models? We investigate

aspects of the climatic response and feedback/sensitivity first in terms of global mean quantities, then zonally averaged quantities, and finally for geographically distributed quantities.

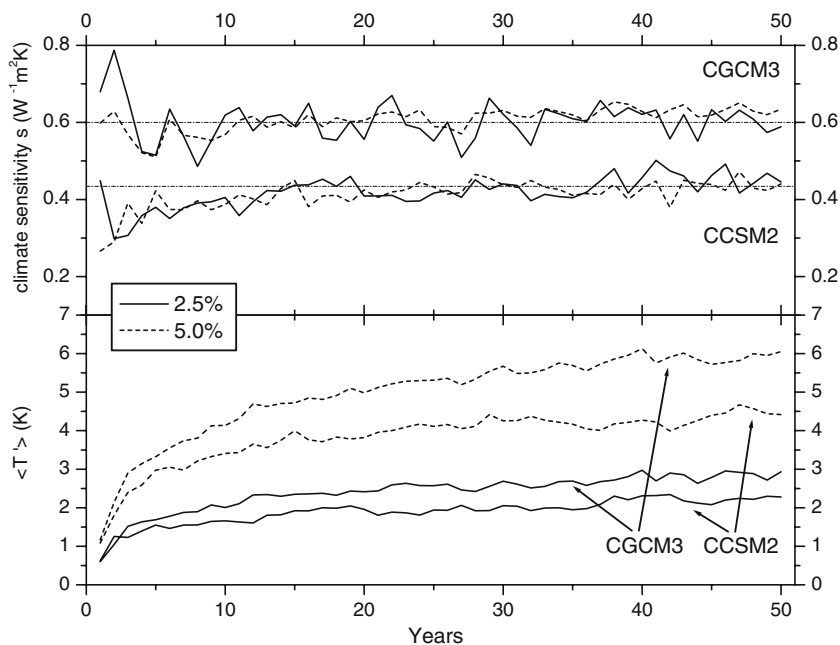
4 Results for global means

Figure 2 displays the time evolution of the global mean temperature response $\langle T' \rangle$ (lower panel) and the climate sensitivity (upper panel) calculated from annual averaged quantities for simulations with imposed solar constant increases of 2.5 and 5%. The calculated climate sensitivities display some variability in the early years but approach a reasonably constant value by the end of about 30 years of integration. The inferred near-equilibrium climate sensitivities, calculated for averages over years 41–50 of the simulations and the associated feedbacks are given in Table 1. This sensitivity of the CCCma model is almost 50% larger than that of the NCAR model and this is reflected in the temperature evolution of Fig. 2.

4.1 Temperature response to volcano-like forcing

Figure 3 displays results for each of the three realizations of the idealized volcano-like perturbation experiment for the two models as well as the ensemble averages. The first column gives results from the CCCma CGCM3, the second column gives results from the NCAR CCSM2 and the third column the ensemble averages across the three simulations for each model.

Fig. 2 The time evolution of the global mean temperature response $\langle T' \rangle$ (lower panel) and the climate sensitivity (upper panel) calculated from annual averaged quantities for simulations with imposed solar constant increases of 2.5 and 5%



The top row of panels displays the temperature response $\langle T' \rangle$, the middle row of panels the global mean volcano-like forcing $\langle f \rangle$ superimposed on the net TOA radiative change $\langle R' \rangle$, and the bottom row of panels the radiative response $\langle g \rangle$.

In the rightmost column, the perhaps surprising result is that the ensemble mean temperature responses of the two models to the volcano-like forcing is very similar, despite the divergence of their temperature responses under constant forcing and the differences in their near-equilibrium climate sensitivities in Fig. 2. This suggests that the global temperature response to a known volcano-like radiative forcing is not, by itself, a robust measure of climate sensitivity in sophisticated coupled climate models and, by implication, for the real climate system.

Yokohata et al. (2005) simulate the global temperature response to a Pinatubo-like volcanic event with two versions of a coupled climate model with different climate sensitivities. They find that the global cooling is larger, and the recovery toward climatology is slower, for the version of the model with the higher climate sensitivity, in apparent contradiction to the temperature results of Fig. 3. However, their two model versions have the same ocean component and, we presume, the same or similar values of κ in (10). In that case the temperature response depends on the feedback/sensitivity of the two versions of the model in the expected way. Nevertheless, is not possible to infer the value of feedback/sensitivity without knowledge of the oceanic heat storage as we will show at some length below.

4.2 Temperature insensitivity

From (8) the difference in the temperature responses of two models with different feedback/sensitivities, but the same forcing, is given to first order by

$$\delta\langle T' \rangle = \frac{\delta\langle dh'/dt \rangle - \langle T' \rangle \delta\hat{\Lambda}}{\hat{\Lambda}} \tag{11}$$

where δX represents the difference between the two model results and $\delta\langle f \rangle \approx 0$. If the temperature responses of the two models are similar, as seen in Fig. 3, then nominally the difference in feedback (the second term in the numerator) must be compensated by a difference in the storage term (which implies a difference in either the depth of the mixed layer or the heat flux into the deep ocean or both).

If the storage term is, as expected, dominated by ocean behaviour then the Yokohata et al. result is not unexpected. For two versions of a model with the same ocean component we might expect the same form of the flux into the deep ocean and the same κ but different $\hat{\Lambda}$ in (9,10) with a difference in temperature response following from the difference in feedback/sensitivity. The implication of (11) and of the “temperature insensitivity” of Fig. 3 is not that different sensitivities have no effect on temperature response but rather that the dependence on feedback/sensitivity is not dominant when the temperature change is small and that the magnitude and nature of the heat storage in the ocean is also important. Finally, we note that the feedback term is not necessarily constant so that the feedback/sensitivity $\hat{\Lambda}(t) = -1/\hat{s}(t)$ for short timescale volcano-like forcing need not be the same as the equilibrium feedback/sensitivity in Fig. 2 and Table 1.

The insensitivity of the temperature response to modest forcing in sophisticated climate models is also seen in simulations of twentieth century climate change collected, for instance, in the various IPCC reports (e.g. IPCC 2001). The forced temperature evolution over the twentieth century agrees rather well among model results despite the models’ different equilibrium climate sensitivities. The simulated temperatures do

Table 1 Near-equilibrium feedback $\hat{\Lambda}$ ($\text{Wm}^{-2} \text{K}^{-1}$) and sensitivity \hat{s} ($\text{KW}^{-1} \text{m}^2$) parameters for constant solar forcing and inferred feedback factors $\hat{\Lambda}_*$ and heat capacities C ($10^8 \text{Jm}^{-2} \text{K}^{-1}$)

both with one standard deviation estimates of uncertainty (in brackets) from the non-linear fit to $\langle T' \rangle$ for known volcano-like forcing $\langle f \rangle$

	CCCma CGCM3			NCAR CCSM2		
Constant forcing	Feedback $\hat{\Lambda}$ and sensitivity (\hat{s})					
2.5% solar	- 1.68 (0.60)			- 2.22 (0.45)		
5.0% solar	- 1.60 (0.63)			- 2.30 (0.43)		
Volcano-like forcing from fit to $\langle T' \rangle$	$\hat{\Lambda}_*(\pm\sigma_{\hat{\Lambda}})$ $s_i = 1$	$\hat{\Lambda}_*(\pm\sigma_{\hat{\Lambda}})$ $s_i = s_e$	$C(\pm\sigma_C)$ $s_i = s_e$	$\hat{\Lambda}_*(\pm\sigma_{\hat{\Lambda}})$ $s_i = 1$	$\hat{\Lambda}_*(\pm\sigma_{\hat{\Lambda}})$ $s_i = s_e$	$C(\pm\sigma_C)$ $s_i = s_e$
Case 1	- 2.20(0.64)	- 3.31(0.02)	2.56(0.05)	- 3.24(1.07)	- 3.46(0.04)	2.54(0.04)
Case 2	- 2.73(0.70)	- 3.33(0.02)	2.38(0.05)	- 3.47(0.96)	- 3.28(0.04)	2.49(0.04)
Case 3	- 3.21(0.81)	- 3.37(0.02)	2.16(0.04)	- 2.52(0.67)	- 3.28(0.04)	2.66(0.04)
Average	- 2.86(0.77)	- 3.35(0.02)	2.36(0.05)	- 3.02(0.88)	- 3.34(0.04)	2.56(0.04)
Mixed-layer ocean	- 1.28(0.20)		2.00(0.04)			

begin to diverge for the twenty-first century as the magnitude of the forcing and of the temperature response both increase.

The reason for this behaviour in simulations of twentieth century warming and, more generally, for the similarity in simulated temperature changes over shorter compared to longer periods is likely a combination of the two mechanisms represented by the terms in the numerator of (11). Boer et al. (2000) suggest that since the twentieth century temperature change $\langle T' \rangle$ is comparatively small this discounts the differences in feedback/sensitivity between models in the $\langle T' \rangle \delta \hat{\Lambda}$ term. The system has not had time to respond to the comparatively weak forcing so the feedback/sensitivity term is not yet controlling. On the other hand, Raper et al. (2002) show that there is some tendency, although it is not consistent across the models studied,

for the storage of heat in the deep ocean to be larger for models with larger sensitivities and argue that this will act to make the shorter timescale transient temperature responses agree. To the extent that these arguments apply to the real system, it argues for the first order difficulty of inferring climate sensitivity using only the temperature response to volcano-like forcing.

4.3 Fitting the temperature curve

The similarity between the temperature responses from the two models subject to the same volcano-like forcing but having different equilibrium climate sensitivities provides *a priori* evidence that it is difficult to infer equilibrium climate sensitivity from the temperature response alone. Nevertheless, it is possible that

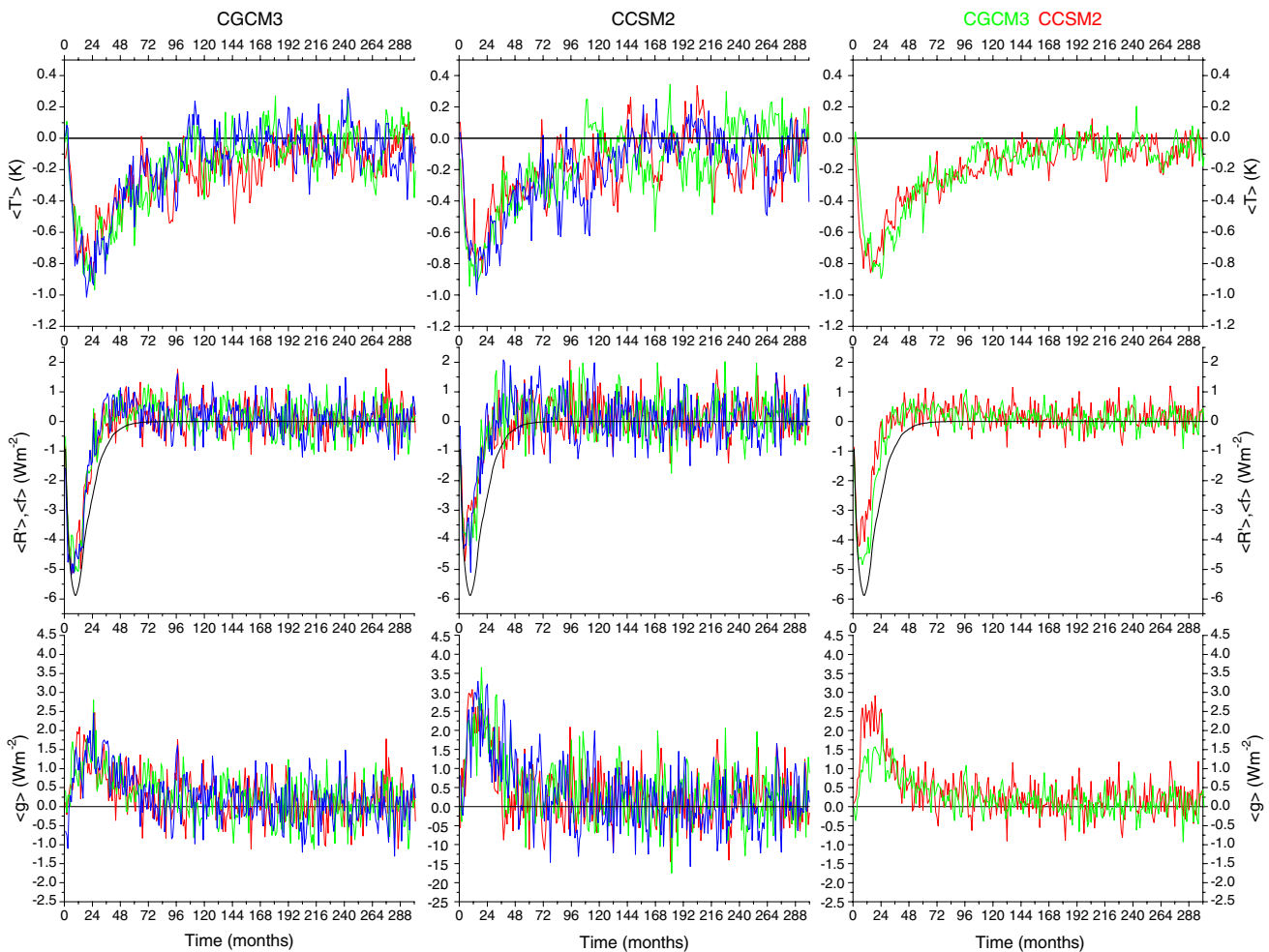


Fig. 3 Results for globally averaged temperature change $\langle T' \rangle$, TOA net radiative flux change $\langle R' \rangle$ and feedback $\langle g \rangle$ where $\langle R' \rangle = \langle g \rangle + \langle f \rangle$ and $\langle f \rangle$ is the radiative forcing. The *first column* gives results from the three individual realizations of the volcano-like perturbation experiment with the CCCma CGCM3

and the *second column* gives results for the NCAR CCSM2. The *third column* gives the ensemble averages across the three realizations for CGCM3 (green) and CCSM2 (red). The global mean forcing $\langle f \rangle$ is the black curve superimposed on the plots of $\langle R' \rangle$ in the *middle row of panels*

there is useful information in the evolution of the temperature response curves. We may fit the “observed” temperature curve(s) of Fig. 3 to the function (10) and infer the parameters (C , Λ_* , f_{\max} , τ) by least squares, although the fitting procedure may not converge if all four parameters are sought. Assuming the parameters (f_{\max} , τ) and the form of the forcing (1) are known (as is the case here although generally not in the case of the real system) we infer the values of (C , Λ_*) by minimizing

$$\chi^2 = \sum_i \left(\frac{\langle T'_i \rangle - \frac{f_{\max}}{C(1-\beta\tau)^2} \{ \tau e^{1-\beta t_i} - (\tau + (1-\beta\tau)t_i) e^{1-t_i/\tau} \}}{s_i} \right)^2 \quad (12)$$

where the sum is over the monthly values of $\langle T'_i \rangle$ in Fig. 3. The minimum is sought using the Levenberg–Marquardt method as embodied in the codes in Numerical Recipes (Press et al. 1992). Here the s_i in the denominator of (12) is a measure of the uncertainty in $\langle T'_i \rangle$. We have a crude estimate of this as s_ε , the scatter among the three realizations in Fig. 3, or we may set $s_i = 1$ whence (12) becomes the usual unweighted least squares. The results of the fitting procedure are given in Table 1 and shown in Fig. 4. Figure 4 also displays the result from a simulation with the CCCma model where the full ocean model is replaced by a “mixed-layer” ocean component. A considerably stronger temperature response is seen for that simulation.

The fitting procedure returns C , $\hat{\Lambda}_*$ and estimates of the uncertainty in terms of a standard deviation ($\pm\sigma$). Table 1 indicates that the most consistent fit is attained when the ensemble scatter s_ε is used to condition the fit as compared to the usual least squares with $s_i = 1$. For this reason we only show the inferred heat capacities for this case. We note, however, that for actual volcanic cases the usual least squares fit would typically be used with the associated greater uncertainty in the inferred values. The immediate result is that the “effective” feedback is considerably more strongly negative (the effective sensitivity is considerably smaller) than the near-equilibrium values for both models, presumably as a consequence of heat penetration into the deep ocean.

For the CCCma model, this is explicit in the mixed-layer ocean simulation where there is no heat penetration into the deep ocean and where the inferred feedback (hence the sensitivity), obtained by fitting to the temperature for the single available simulation, is much closer to the equilibrium feedback/sensitivity values than is the case for the fully coupled model. The inferred heat capacity of $2.00(0.04) \times 10^8 \text{ Jm}^{-2} \text{ K}^{-1}$ is

also very close to the value of $C = \rho C_0 \Delta z = 1,025 \times 3,990 \times 50 = 2.04 \times 10^8 \text{ Jm}^{-2} \text{ K}^{-1}$ appropriate to the 50 m depth of the mixed layer in the slab ocean case. For the full ocean cases the inferred heat capacity is typically larger than this and the value for the NCAR model is modestly larger than that of the CCCma model. The overall conclusion is that climate sensitivity cannot be inferred directly from the global average temperature response to volcano-like forcing even if the forcing is known. An independent knowledge of the heat penetration into the deep ocean is required.

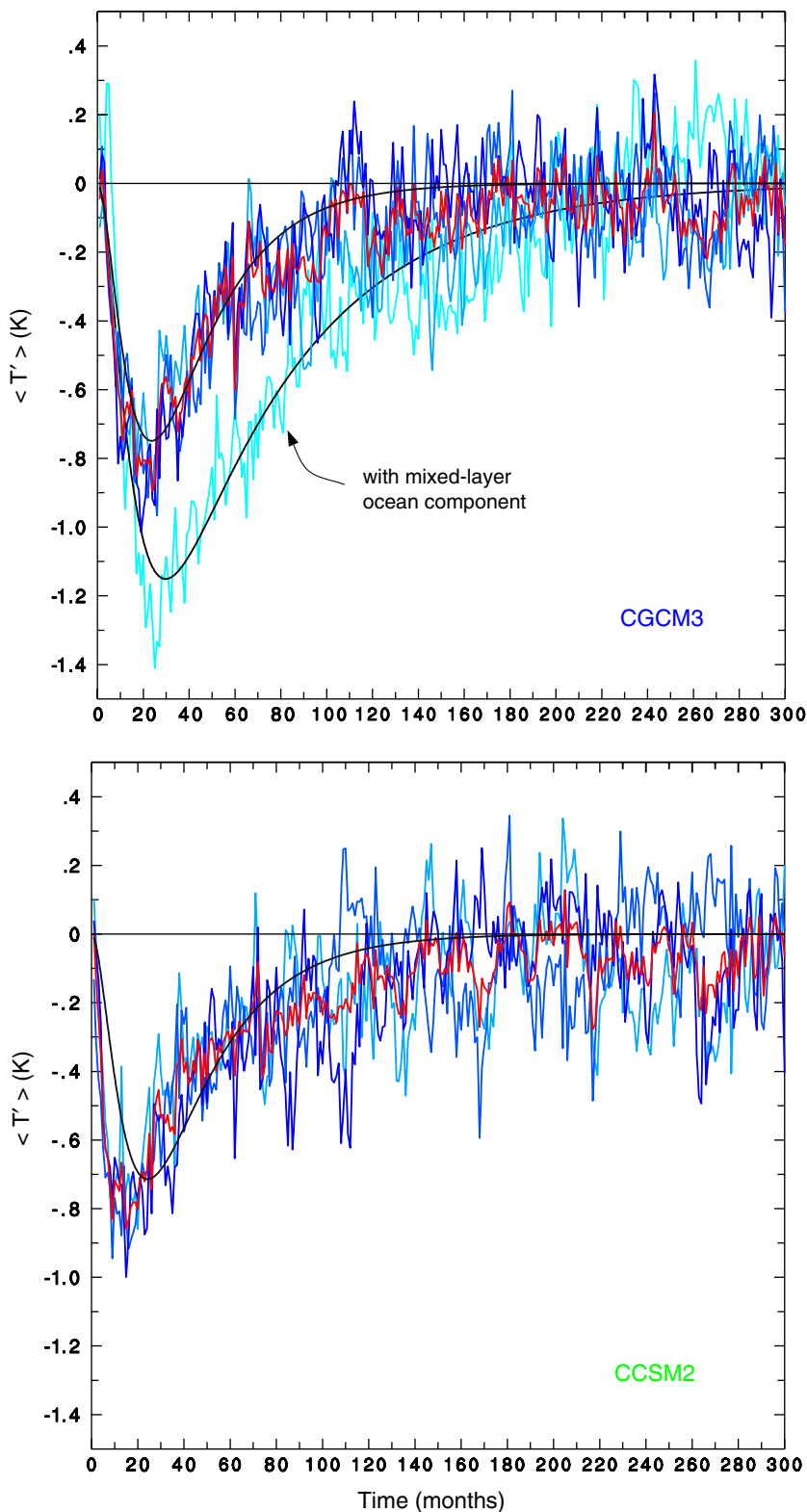
One possibility is that this heat penetration is small in the real climate system so that it operates in a manner similar to the mixed-layer ocean model (rather than the full ocean model) so that a reasonably correct value of feedback/sensitivity can be inferred from the temperature response alone. This is argued by Douglass and Knox (2005b, c) in response to comments by Wigley et al. (2005a, b) and Robock (2005) on an earlier paper (Douglass and Knox 2005a) in which a strong negative climate feedback (hence weak climate sensitivity) is inferred based on the temperature response to the Mount Pinatubo eruption.

The rate of heat penetration into the deep ocean is difficult to obtain accurately from observations, particularly over the relatively short period involved in a volcanic event. A number of studies argue that the trend in observation-based oceanic heat content changes are consistent with those simulated in models of the climate system in the context of climate change (e.g. Levitus et al. 2001; Barnett et al. 2001; Sun and Hansen 2003). Gregory et al. (2004) argue that superimposed decadal variability is not well simulated, however, and suggest that analysis results may be sensitive to assumptions made for data sparse regions. They urge caution in comparing model variability results with those from ocean analyses.

Church et al. (2005) compare the results of simulations of twentieth century climate made with a number of climate models that include representations of volcanic forcing with observation-based analyses of upper ocean heat content and mean sea-level (Levitus et al. 2005; Ishii et al. 2003). They conclude that large volcanic eruptions produce a rapid reduction in ocean heat content and mean sea-level and that there is qualitative agreement between model simulated and observation-based values of global mean ocean heat content and sea-level for the period 1960–2000.

All of this indicates that a knowledge of the temperature response alone is not sufficient to allow the climate sensitivity to be obtained even if volcanic forcing is perfectly known. The ocean heat storage

Fig. 4 Individual (blue) and ensemble mean (red) temperature responses to volcano-like forcing for the CCCma CGCM3 (upper panel) and the NCAR CCSM2 (lower panel) coupled atmosphere-ocean models. The light blue curve in the upper panel is for a simulation where the ocean component of the coupled model is replaced by a “mixed-layer” or “slab” ocean component which allows no heat exchange with the deep ocean. The smooth black lines are the non-linear least squares best fits of the analytic function (10) to the ensemble mean temperature responses



term cannot be neglected either for the real system nor for the current generation of sophisticated coupled models such as those included in the IPCC Assessment. A sufficiently accurate estimate of the heat storage

term is a necessary condition to allow an accurate estimate of climate sensitivity. It remains to be determined if sensitivity can be reliably estimated even when this heat storage term is known,

4.4 Feedback/sensitivity when system heat storage is known

Assuming a knowledge of the volcanic forcing and the heat storage we may appeal to the globally averaged budget (7) in the form

$$\hat{\Lambda} = \frac{\langle dh'/dt - f \rangle}{\langle T' \rangle} = \frac{\langle R' - f \rangle}{\langle T' \rangle} = \frac{\langle g \rangle}{\langle T' \rangle} \quad (13)$$

in order to infer the feedback/sensitivity. The heat storage term is potentially available from oceanic observations (presuming the storage in the atmosphere and land may be neglected) although there are practical difficulties as discussed in Sect. 4.3. Satellite measurements of the TOA radiation $\langle R' \rangle$ offer an alternative and perhaps more achievable path to the storage term.

Each of the quantities in (13) is a combination of the forced volcanic signal and unforced natural variability. Even if we know the quantities themselves we are faced with separating the signal from the noise in order to infer the climate feedback/sensitivity. The most obvious approach is to average the quantities over some time period and to estimate $\hat{\Lambda}$ from the averages. Figure 5 gives monthly “cumulative” estimates of the feedback and the sensitivity which are obtained by averaging from the beginning of the forcing to some time τ^* as

$$\Lambda(\tau^*) \approx \frac{\int_0^{\tau^*} \langle g \rangle dt}{\int_0^{\tau^*} \langle T' \rangle dt} \approx -1/s(\tau^*). \quad (14)$$

Results from the three individual volcano-like simulations and their ensemble average are plotted as are the result from the simulation with a constant 2.5% increase in the solar constant. The result from the version of CGCM3 with a slab/mixed-layer ocean component is also plotted. The initial 12 monthly values are not plotted since they are dominated by noise but the results begin to stabilize thereafter. However, the estimates of $\Lambda(\tau^*)$ from individual volcano-like simulations tend to “wander” while the ensemble mean result approaches a reasonably constant value. This points out the difficulty in arriving at an optimum averaging period given the transient nature of the signal and the superimposed natural variability “noise” in both components of (14). In particular, if $\langle g \rangle = g_s + g_*$ and $\langle T' \rangle = T'_s + T'_*$ indicate signal and noise components then (14) becomes

$$\Lambda(\tau^*) = \frac{\int_0^{\tau^*} g_s dt + \int_0^{\tau^*} g_* dt}{\int_0^{\tau^*} T'_s dt + \int_0^{\tau^*} T'_* dt} \quad (15)$$

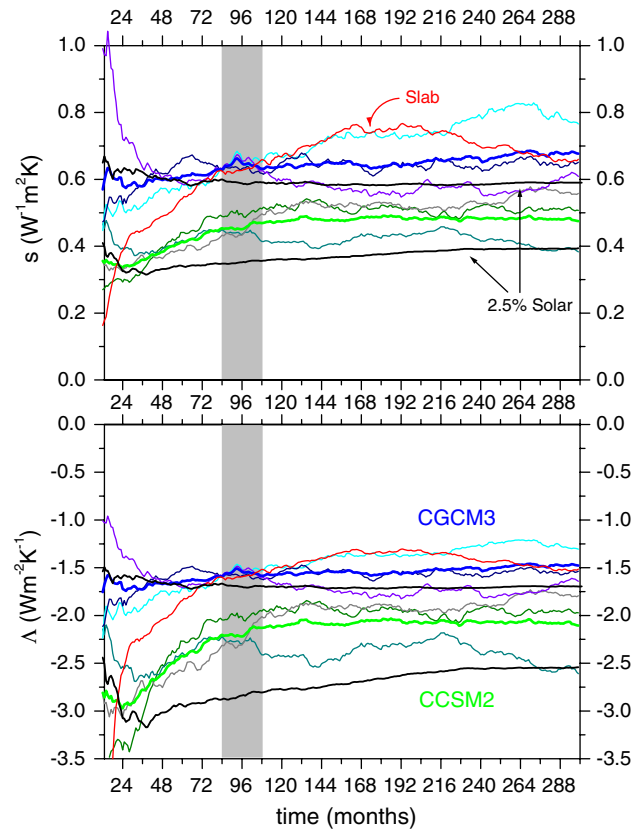


Fig. 5 Monthly cumulative estimates of the climate sensitivity \hat{s} and global feedback $\hat{\Lambda}$ terms obtained from $\Lambda(\tau^*) = \int_0^{\tau^*} \langle g \rangle dt / \int_0^{\tau^*} \langle T' \rangle dt = -1/s(\tau^*)$, i.e. by averaging the radiative and temperature response terms from the beginning of the volcano-like forcing to some time τ^* . The blue lines give the results from the three realizations for CGCM3 and the thick blue line the ensemble average result. The green lines give the corresponding results for CCSM2. The grey band indicates a range of averaging times τ^* of around 8 years for which the values of $s(\tau^*)$ and $\Lambda(\tau^*)$ tend to converge. Values subsequently diverge as a consequence of averaging over the natural variability after the volcano signal has diminished. Black lines give the results for simulations with an imposed 2.5% increase in the solar constant. Finally, the red lines are the result for the volcano-like experiment with the slab/mixed-layer ocean version of CGCM3

For the volcano-like simulations, the numerator and denominator are the areas under the curves in Fig. 3 for $\langle T' \rangle$ and $\langle g \rangle$ and that figure gives a qualitative sense of the signal and noise components.

Figure 5 indicates that the estimate of the feedback/sensitivity for an individual volcano-like forcing simulation does not stabilize with increasing averaging time. The reason for this has to do with the integration of the noise term. As averaging time increases, the integral of the signal component approaches a constant value comparatively rapidly. The value of the integrated signal component does not change for longer integra-

tion times since the signal itself has returned to zero and no longer contributes to the integral.

The situation is somewhat different for the noise term and its integral will wander about zero. Thus, for $\int_0^{\tau^*} g_* dt \approx \sum_{t=1}^{\tau^*} g_*(t)$ if we consider the expected value of the mean square deviation of the noise integral from zero we have

$$E\left(\sum_{t=1}^{\tau^*} g_*(t)\right)^2 = E\sum_{t=1}^{\tau^*} \sum_{l=1}^{\tau^*} g_*(t)g_*(l) = \sigma_{g_*}^2 \tau^*(1+b) \quad (16)$$

where σ_{g_*} is the noise variance and $b = 2\sum_{l=1}^{\tau^*-1} (1-l/\tau^*)r(l)$ depends on the autocorrelation structure of the noise where $r(l)$ are autocorrelations at lag l . If the autocorrelations are zero at all lags, $b = 0$ and (16) becomes $\sigma_{g_*}^2 \tau^*$ but this will not be the case for the variables considered here and we expect $b > 0$. The expected deviation of the noise integral from zero, in the root mean square sense, is $d = \sigma_{g_*} \sqrt{\tau^*(1-b)}$ which increases with integration time τ^* . We express this symbolically as

$$\Lambda(\tau^*) = \frac{\int_0^{\tau^*} g_s dt + \int_0^{\tau^*} g_* dt}{\int_0^{\tau^*} T'_s dt + \int_0^{\tau^*} T'_* dt} \rightarrow \frac{\tilde{g}_s \pm \sigma_{g_*} \sqrt{\tau^*(1-b)}}{\tilde{T}'_{*s} \pm \sigma_{T_*} \sqrt{\tau^*(1-b)}}, \quad (17)$$

where $\tilde{g}_s, \tilde{T}'_s$ are the contributions to the integral from the signal component and the remaining terms the contribution to the integral from the noise component, to indicate this behaviour.

The message of (17) is that the integral of the signal components become constant as averaging time increases while the integral of the natural variability

noise is not expected to approach more and more closely to zero as averaging time increases. Rather, the integral of the noise may be expected to deviate from zero by an amount roughly proportional to the square root of the averaging time. This implies that the optimum estimate of feedback/sensitivity would be obtained by a comparatively short averaging time that captures the signal but does not integrate over the noise when the signal is small. Figure 3 suggests that a suitable averaging period might be of the order of 8–10 years, or even less, and Fig. 5 indicates how the results from the three volcano-like simulations tend to converge at around the 8 year averaging period (the shaded grey band) and then drift apart again. The ensemble average result, where the noise is at least partially averaged out, approaches a comparatively stable value at about this integration time.

The situation is quite different for constant forcing as illustrated by the 2.5% solar cases which are the black lines in Fig. 5. Here the signal components attain a constant value as equilibrium is approached and their integrals grow with the integration time as τ^* , i.e. faster than the noise term, and longer integration improves the estimate. This qualitative behaviour is apparent in Fig. 5 where feedback/sensitivities for the 2.5% solar constant case rapidly approach a reasonably constant value for CGCM3 and a smoothly increasing value for CCSM2. By contrast, results from the three volcano-like simulations wander apart at longer averaging times. Thus, even if the forcing and heat storage are known for a particular volcano, the volcanic signal is at least partially obscured by the noise and this adds uncertainty to the estimate of feedback/sensitivity.

Table 2 Global mean values of the feedback parameter and its components $\hat{\Lambda} = \hat{\Lambda}_L + \hat{\Lambda}_S = \hat{\Lambda}_A + \hat{\Lambda}_C = \hat{\Lambda}_{LA} + \hat{\Lambda}_{LC} + \hat{\Lambda}_{SA} + \hat{\Lambda}_{SC}$ for CGCM3 diagnosed from year 41 to 50 averages for the 2.5 and 5% solar constant increase experiments and from 8 year averages of the ensemble mean of three volcano-like experi-

ments. Associated mean square differences and spatial correlation statistics give measures of quantitative agreement between the geographical patterns of the feedbacks for the volcano-like transient and constant 2.5% solar increase simulations. Units are ($Wm^{-2} K^{-1}$)

	$\hat{\Lambda}$	$\hat{\Lambda}_S$	$\hat{\Lambda}_L$	$\hat{\Lambda}_A$	$\hat{\Lambda}_C$	$\hat{\Lambda}_{SA}$	$\hat{\Lambda}_{SC}$	$\hat{\Lambda}_{LA}$	$\hat{\Lambda}_{LC}$
Global means									
2.5%	-1.68	0.78	-2.46	-1.75	0.07	0.67	0.11	-2.42	-0.04
5%	-1.60	0.79	-2.39	-1.68	0.09	0.70	0.09	-2.39	-0.00
Volcano	-1.54	0.83	-2.37	-1.52	-0.02	0.94	-0.11	-2.46	0.09
Mean square differences $\langle d^2 \rangle = \langle d \rangle^2 + \langle [d]^{+2} \rangle + \langle d^{*2} \rangle$									
$\langle d \rangle^2$	0.02	0.00	0.01	0.05	0.01	0.07	0.05	0.00	0.02
$\langle [d]^{+2} \rangle$	0.16	0.39	0.35	0.41	0.18	1.03	0.43	0.31	0.13
$\langle d^{*2} \rangle$	3.92	5.95	4.12	3.37	3.57	4.39	5.53	1.33	2.15
Spatial correlations $(r, r_+, r_*) = \left(\frac{\langle X^+ Y^+ \rangle}{\sigma_X \sigma_Y}, \frac{\langle [X]^+ [Y]^+ \rangle}{\sigma_{[X]^+} \sigma_{[Y]^+}}, \frac{\langle X^* Y^* \rangle}{\sigma_{X^*} \sigma_{Y^*}} \right)$									
r	0.41	0.31	0.21	0.59	0.38	0.65	0.41	0.55	0.21
r_+	0.89	0.55	0.74	0.88	0.88	0.88	0.86	0.89	0.80
r_*	0.28	0.28	0.05	0.46	0.21	0.52	0.23	0.32	0.06

The top two rows of Tables 2 and 3 give global mean values of the feedback parameter and its components, following (5), based on years 41–50 averages of the 2.5 and 5% solar constant simulations for CGCM3 and CCSM2. The third row of the tables gives estimates of these quantities for the average of the three volcano-like simulations from (14) where the averaging is over months 1–96. Tables 2 and 3 indicate that if both the forcing and the heat storage are known the equilibrium climate feedback/sensitivity of the modelled system (and by inference the real system) may be estimated to reasonable accuracy from strong volcano-like perturbations. For both models the volcano-based sensitivity estimate is slightly higher than the near-equilibrium value inferred from the 2.5 and 5% solar forcing cases.

Figure 5 also shows a difference in behaviour in the evolution of feedback/sensitivity for the 2.5 and 5% solar constant experiments between the models (which is also apparent in Fig. 2). The CGCM3 value approaches its near-equilibrium value much more rapidly than does the CCSM2 value, for which the feedback/sensitivity evolves and increases with time. The somewhat paradoxical result for CCSM2 is that the estimates of feedback/sensitivity based on the volcano and solar constant simulations differ noticeably in the shaded band around 96 months in Fig. 5 but they agree very well in Table 3.

The results of Fig. 5 and Tables 2 and 3 indicate that volcano-like perturbations to the system can provide a first order estimate of the equilibrium climate sensitivity and are able to distinguish between the differing climate sensitivities of the two models. In other words, our experiments support the possibility of inferring the climate sensitivity of the real system by studying the

impact of volcanoes provided, however, that both the forcing and the heat storage in the system are known with sufficient accuracy.

4.5 Consequences of error in forcing and heat storage

From (14), errors in forcing and heat storage are combined in errors of $\langle g \rangle = \langle dh'/dt - f \rangle$ and a general idea of the consequences of error may be obtained from

$$\frac{\delta\Lambda}{\Lambda} = \frac{\frac{1}{\tau^*} \int_0^{\tau^*} \delta\langle g \rangle dt}{\frac{1}{\tau^*} \int_0^{\tau^*} \langle g \rangle dt} - \frac{\frac{1}{\tau^*} \int_0^{\tau^*} \delta\langle T' \rangle dt}{\frac{1}{\tau^*} \int_0^{\tau^*} \langle T' \rangle dt} \tag{18}$$

where Fig. 6 displays the denominators of each of the right-hand terms as a function of the integration time τ^* . To estimate the global feedback/sensitivity to within 25% requires the percent errors in each of the integrals of g and T' be no bigger than this (and smaller if the error terms are of opposite sign). For the integration time of the order of 8 years (the shaded grey band) the denominators are approximately 0.7 W m^{-2} and -0.5 C , respectively, which implies that errors in the numerators must be less than 0.18 W m^{-2} and 0.13 C individually and jointly, even for a strong volcano-like perturbation, if errors in Λ are to be less than 25%.

4.6 Feedback mechanisms

The global feedback may be decomposed into components representing different radiative aspects of the response to the volcano-like perturbation (see Eqs. 5, 6). The subscripts of the nine components

Table 3 Global mean values of the feedback parameter and its components $\hat{\Lambda} = \hat{\Lambda}_L + \hat{\Lambda}_S = \hat{\Lambda}_A + \hat{\Lambda}_C = \hat{\Lambda}_{LA} + \hat{\Lambda}_{LC} + \hat{\Lambda}_{SA} + \hat{\Lambda}_{SC}$ for CCSM2 diagnosed from year 41 to 50 averages for the 2.5 and 5% solar constant increase experiments and from 8 year averages of the ensemble mean of three volcano-like experiments.

	$\hat{\Lambda}$	$\hat{\Lambda}_S$	$\hat{\Lambda}_L$	$\hat{\Lambda}_A$	$\hat{\Lambda}_C$	$\hat{\Lambda}_{SA}$	$\hat{\Lambda}_{SC}$	$\hat{\Lambda}_{LA}$	$\hat{\Lambda}_{LC}$
2.5%	-2.22	0.01	-2.22	-1.34	-0.88	0.82	-0.82	-2.16	-0.06
5%	-2.30	-0.10	-2.20	-1.36	-0.94	0.76	-0.86	-2.12	-0.08
Volcano	-2.19	0.16	-2.36	-1.31	-0.88	0.94	-0.78	-2.25	-0.10
Mean square differences $\langle d^2 \rangle = \langle d \rangle^2 + \langle [d]^{+2} \rangle + \langle d^{*2} \rangle$									
$\langle d \rangle^2$	0.00	0.03	0.02	0.00	0.00	0.01	0.00	0.01	0.00
$\langle [d]^{+2} \rangle$	0.49	0.76	0.82	0.53	0.40	1.32	0.63	0.43	0.26
$\langle d^{*2} \rangle$	7.14	8.26	7.45	4.31	6.31	5.21	8.45	1.55	4.49
Spatial correlations $(r, r_+, r_*) = \left(\frac{\langle X^+ Y^+ \rangle}{\sigma_X \sigma_Y}, \frac{\langle [X]^+ [Y]^+ \rangle}{\sigma_{[X]^+} \sigma_{[Y]^+}}, \frac{\langle X^* Y^* \rangle}{\sigma_{X^*} \sigma_{Y^*}} \right)$									
r	0.50	0.40	0.36	0.58	0.45	0.58	0.36	0.40	0.39
r_+	0.87	0.81	0.51	0.88	0.83	0.80	0.79	0.65	0.78
r_*	0.38	0.26	0.33	0.41	0.36	0.42	0.22	0.26	0.32

Associated mean square difference and spatial correlation statistics give measures of quantitative agreement between the geographical patterns of the feedbacks for the volcano-like transient and constant 2.5% solar increase simulations. Units are ($\text{Wm}^{-2} \text{ K}^{-1}$)

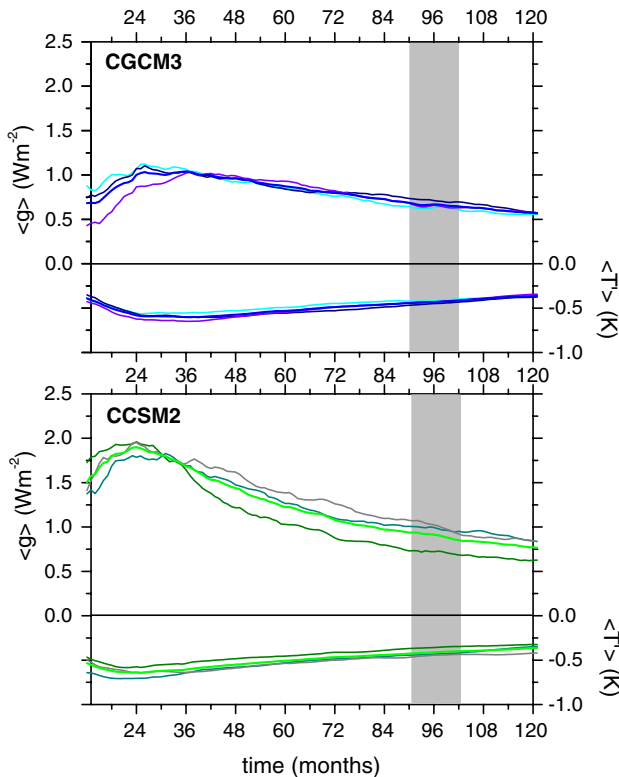


Fig. 6 The integrated quantities $\frac{1}{\tau^*} \int_0^{\tau^*} \langle g \rangle dt$ and $\frac{1}{\tau^*} \int_0^{\tau^*} \langle T' \rangle dt$ for the models. The *thick line* is the ensemble mean and the *thin lines* the individual realizations. The *grey band* indicates the results for the averaging period τ^* of around 8 years

$\Lambda = \Lambda_L + \Lambda_S = \Lambda_A + \Lambda_C = \Lambda_{LA} + \Lambda_{LC} + \Lambda_{SA} + \Lambda_{SC}$ indicate longwave, shortwave, clear-sky atmosphere/surface, and cloud feedback components.

Figure 7 displays the values of Λ_{LA} , Λ_{LC} , Λ_{SA} , Λ_{SC} as a function of integration time τ^* calculated in the manner of (14). The long and shortwave atmosphere/surface feedbacks are the predominant mechanisms. Solar cloud feedback Λ_{SC} plays a distinctly secondary role in CGCM3 but is an important negative feedback in the CCSM2 model. The two models also differ in how this component behaves in response to volcano-like and constant forcing. For volcano-like forcing Λ_{SC} is less negative than for the constant forcing in CCSM2 while the reverse is the case for the CGCM3. The remaining feedback components behave similarly for the two models so that the overall difference in the feedback/sensitivity between them depends on the difference in the shortwave cloud feedback. This is also a conclusion of the Stowasser et al. (2006) analysis.

5 Geographical aspects

In Sect. 4 the overall behaviour of globally averaged quantities for the volcano-like simulations is seen to be

reasonably similar to near-equilibrium results. The zonal and geographical aspects of the response may also be investigated to see if this agreement holds more generally. In order to minimize the effect of natural variability noise we consider the average of the three realizations of the volcano-like experiment.

5.1 Temperature

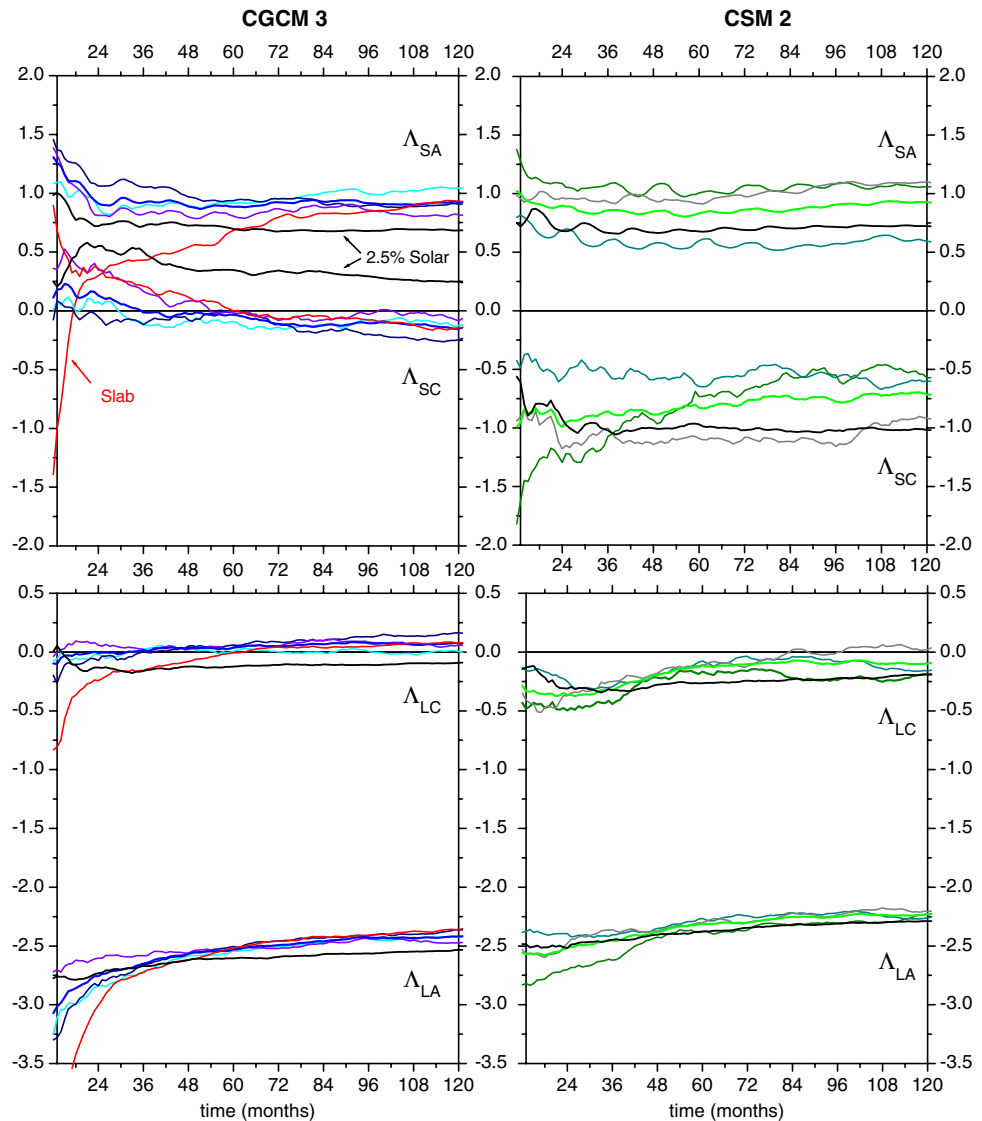
In addition to the global mean temperature anomalies discussed previously, Robock and Mao (1995) consider zonally averaged temperature anomalies for a composite of the six largest volcanoes of the past century. Their anomalies are calculated with respect to the mean of the 5-year period preceding the eruption. The analogous results for the composite of three volcano-like simulations from each model are shown in Fig. 8 where here the anomalies are calculated with respect to the models' control simulations.

The results generally resemble those Fig. 6 of Robock and Mao (1995) up to and including the broad cooling following the “eruption” with maximum cooling in the two Northern Hemisphere summers following the volcano and with some evidence of warming in the high latitude northern winters. The amplitude of the response in Fig. 8 is larger than that found in Robock and Mao due to the consistency and comparatively strong forcing of the volcano-like perturbations. The qualitative agreement of the pattern of the response with the observation-based result argues for the generality of the response and its broad independence from the details of the forcing.

Figure 9 displays the geographic pattern of temperature responses for the two models averaged over months 7–42 of the simulations which is the 3 year period for which the temperature response generally exceeds one half its maximum value. The notable similarity of the global mean temperature responses of the two models in Fig. 4 is a consequence of the qualitative similarity of both the amplitude and geographic patterns of temperature responses for the two models. Since the forcing is negative the overall result is a cooling although there are regions of modest warming at high latitudes. The patterns are similar to those exhibited by these models in global warming simulations, although of the opposite sign, in keeping with the idea that the pattern of the feedbacks largely determines the pattern of temperature response rather than the pattern or sign of the forcing itself (Boer and Yu 2003a).

Figure 8 gives some indication that volcano-like forcing may result in subsequent high latitude winter warming, at least for CGCM3. Observational charac-

Fig. 7 Monthly cumulative estimates of the feedback components Λ_{LA} , Λ_{LC} , Λ_{SA} , Λ_{SC} , respectively the longwave clear-sky and cloud feedbacks and corresponding shortwave clear-sky and cloud feedbacks, for the two models. The quantities are functions of the integration time τ^* and the colours correspond to those of Fig. 5

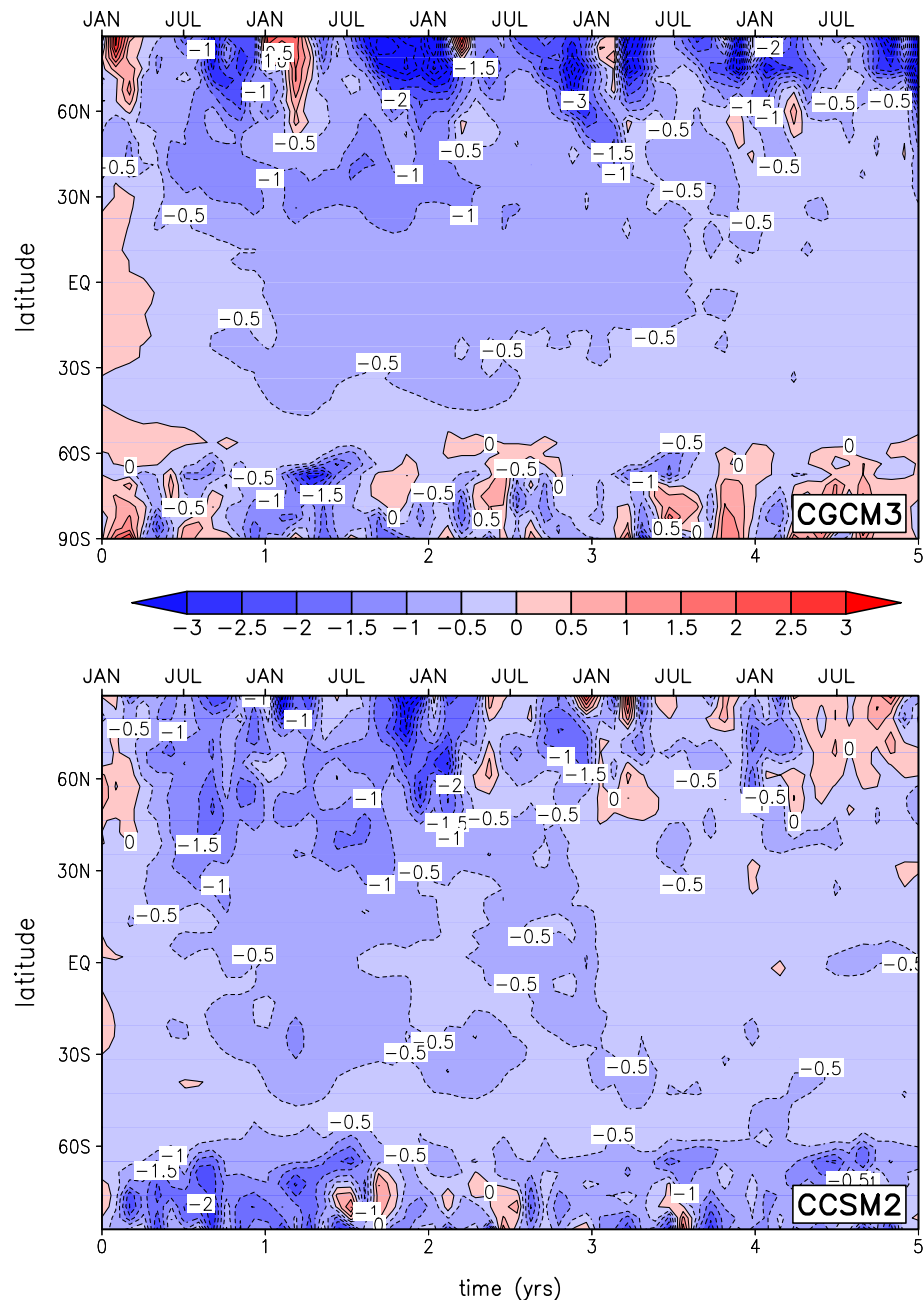


terizations of this somewhat counter-intuitive behaviour include those of Robock and Mao (1995) and Stenchikov et al. (2006) which includes also references to a range of past studies. Although the composites produced include different volcanoes and different times following the eruptions they are linked by the common feature of enhanced post-volcano winter warming over northern Eurasia. Stenchikov et al. (2006) compare the composite responses of nine volcanic events in seven climate models in simulations of past climate from 1850 to the present and report that the winter warming response is not consistent across models and is generally weaker than that inferred from observations.

Figure 10 displays the temperature difference between the first and second northern winters following the onset of the volcano-like forcing for the CCCma model. There is some indication of a winter

warming result for this model but no evidence of this response in the NCAR model (which is consistent with the results for this model in Stenchikov et al. for aerosol driven volcano forcing). According to Robock (2000) the heating of the lower stratosphere by the volcanic aerosol produces an enhanced pole to equator temperature gradient and the strengthened polar vortex traps the wave energy of the AO/NAO resulting in winter surface warming. Since the volcano-like forcing imposed here does not produce the kind of stratospheric warming caused by volcanic aerosols this aspect of the forcing is absent in our experiments. It is nevertheless tempting to speculate that post-volcano Eurasian winter warming is at least partially a transient response to broad negative forcing rather than to the details of stratospheric warming/surface cooling in aerosol forced volcano cases (Stenchikov et al. 2002).

Fig. 8 Anomalies of the zonally averaged temperature [T'] following the onset of the volcano-like forcing for the CGCM3 (upper panel) and CCSM2 (lower panel). Units: K

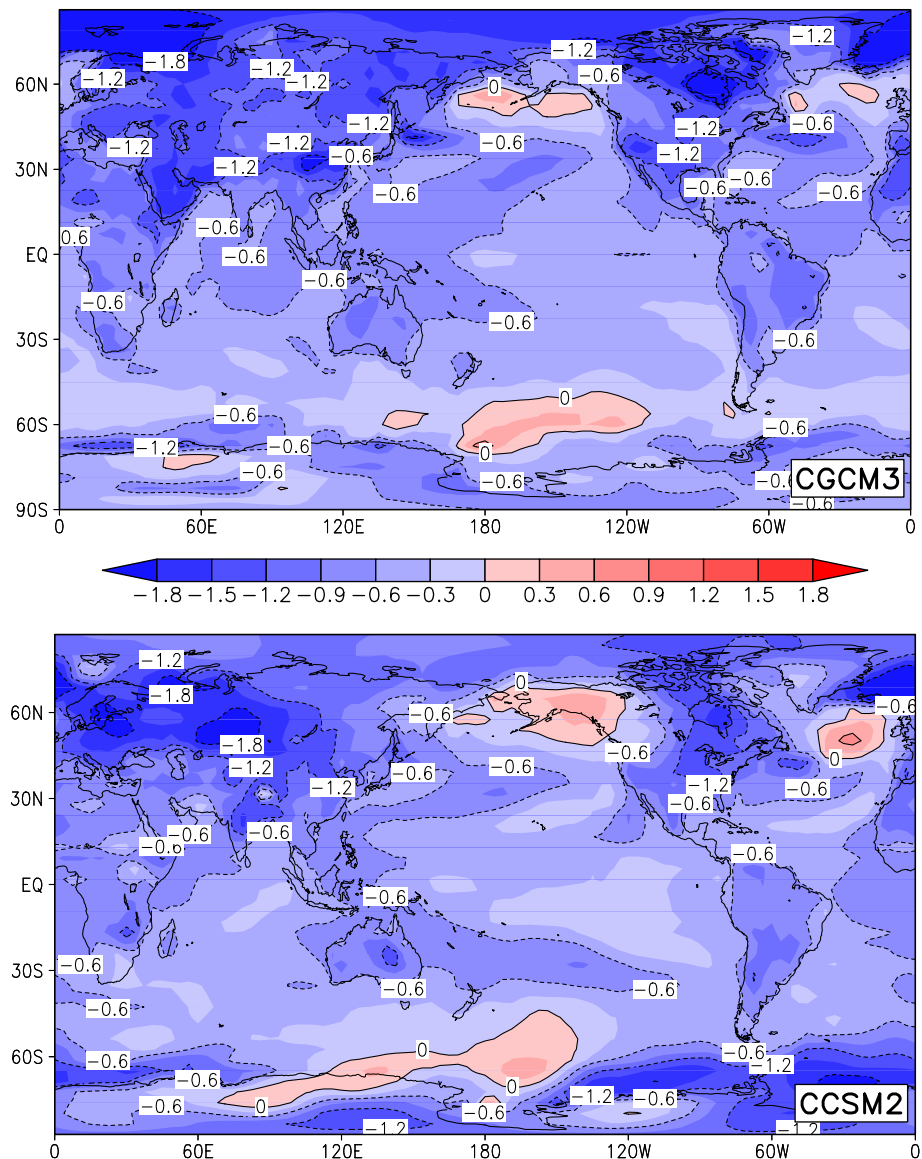


5.2 Feedbacks

The zonal mean of the feedback parameter [Λ] and all eight of its components [Λ] = [Λ_L] + [Λ_S] = [Λ_A] + [Λ_C] = [Λ_{LA}] + [Λ_{LC}] + [Λ_{SA}] + [Λ_{SC}] are plotted in Fig. 11 for the two models, both for the average of the volcano-like simulations and for the near-equilibrium 2.5% solar constant increase simulations. For the volcano-like simulations the average is over the 8 years following the onset of the volcano-like forcing (as suggested by the discussion in Sect. 4.4). For the simulations with increased solar constant, the average

is over years 41–50 of the simulations. As noted in Stowasser et al. (2006) the difference between the overall feedback of the two models occurs mainly at tropical latitudes and is largely associated with the difference in the solar cloud feedback in the models. The purpose of Fig. 11 is to compare the feedback structures obtained for the short-term transient volcano-like forcings with long-term near equilibrium results. It is apparent that the zonally averaged results are generally similar, indicating that the feedback processes are reasonably robust across the different forcing/response timescales.

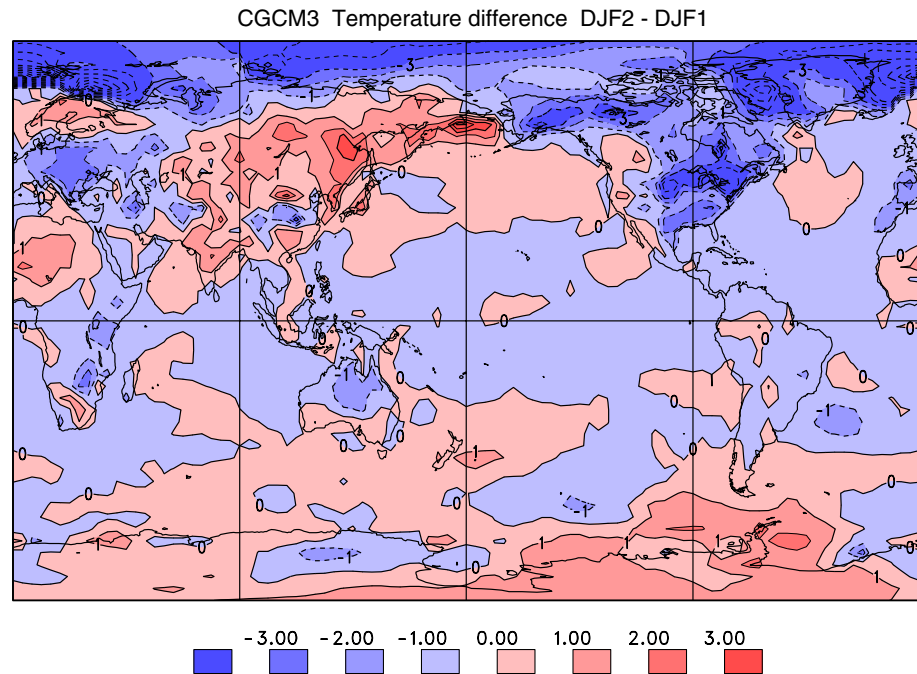
Fig. 9 The temperature response to volcano-like forcing as simulated by the CGCM3 (*upper panel*) and CCSM2 (*lower panel*) models. The response is the average over the first 8 years of the simulations. Units: K



Figures 12 and 13 display the geographical patterns of the feedback and its components diagnosed from the 2.5% solar constant increase simulation (upper panels) and for the volcano-like forcing experiment (lower panels) for the CGCM3 and CCSM2 models respectively, calculated in the same fashion as for Fig. 11. To first order, the geographical patterns of the feedbacks in the transient volcano-like and in the near-equilibrium cases are similar, although the results from the volcano-like experiments are noisier as a consequence of the overall weaker forcing and the shorter adjustment time. Although there is a broad similarity in these geographical patterns of feedback they are by no means identical and feedbacks apparently do operate somewhat differently geographically in response to short term transient forcing compared to long term constant forcing.

Tables 2 and 3 provide quantitative measures of the agreement between these feedback patterns. Decomposing a field X into its global mean $\langle X \rangle$, the north-south structure about the mean $[X]^+ = [X] - \langle X \rangle$, and the remaining geographical pattern $X^* = X - [X]^+$ allows the quantification of the difference $d = Y - X$ between two fields in terms of mean square differences of these components as $\langle d^2 \rangle = \langle d \rangle^2 + \langle [d]^+{}^2 \rangle + \langle d^{*2} \rangle$ and in terms of spatial correlations with $(r, r_+, r_*) = \left(\frac{\langle X^+ Y^+ \rangle}{\sigma_X \sigma_Y}, \frac{\langle [X]^+ [Y]^+ \rangle}{\sigma_{[X]^+} \sigma_{[Y]^+}}, \frac{\langle X^* Y^* \rangle}{\sigma_{X^*} \sigma_{Y^*}} \right)$. The Tables show that the visual agreement between the patterns resides largely in the north-south structures of Figs. 12 and 13 (displayed explicitly in Fig. 11) and less in the geographical patterns that remain after these structures are subtracted out. The best overall agreement between the components is for the clear-sky solar feedback

Fig. 10 The temperature difference between the first and second northern winters (December–February) following the onset of the volcano-like forcing for the CCCma model. Units: K



Λ_{SA} associated with the ice/snow albedo feedback mechanism as might be expected. Clear-sky feedbacks are in better agreement than cloud feedbacks which, as usual, are the least well behaved.

6 Summary

The “climate sensitivity” of the earth system, or of a model of the system, may be characterized by the value of \hat{s} in the relation $\langle T' \rangle = \hat{s} \langle f \rangle$ where $\langle T' \rangle$ is the equilibrium global mean temperature response to the global mean radiative forcing $\langle f \rangle$. The climate sensitivity gives a basic first order measure of the responsiveness of the climate system to a forcing agent such as an increase in the atmospheric concentration of greenhouse gases. If the earth’s climate sensitivity is low, strong forcing will result in only modest climate change and if climate sensitivity is high, even comparatively weak forcing will engender appreciable changes in climate. The earth’s climate sensitivity is a key parameter in understanding the consequences of anthropogenic emissions of greenhouse gases, land use changes and other natural and anthropogenic perturbations to the radiative balance of the climate system. Nevertheless, the earth’s climate sensitivity is not well known.

Modern coupled climate models are used to investigate the past and current workings of the earth’s climate system and to make projections of potential future climate change associated with natural and

anthropogenic forcing. The models are developed from physical first principles in that they are based on the equations of fluid dynamics, thermodynamics, radiative transfer etc. including representations of physical processes such as cloud and precipitation formation, boundary layer processes and so on. The climate sensitivities of the models are not input as parameters but arise as consequence of the interactions simulated in the model and flow from its structure and its representation of the physical processes. Although current coupled models are based on the physical processes operating in the climate system, and despite a considerable history of development, testing and intercomparison, the resulting model climate sensitivities can differ by as much as a factor of two and do not provide a definitive value for the earth’s climate sensitivity.

Given this ambiguity in the climate sensitivity from models it is natural to ask if the earth’s climate sensitivity can be inferred from observed perturbations to it. The climate perturbations associated with large volcanic events are an obvious and much cited possibility. However, the inference of the climate sensitivity from a volcanic event is not a trivial exercise and may not even be possible. Our investigation asks if the equilibrium climate sensitivity of a system like the earth’s can be inferred from a short timescale volcano-like perturbation and, if it is possible, what information is required and to what accuracy must it be known.

Two modern coupled climate models having different climate sensitivities but forced with the same volcano-like radiative forcing are used in the investigation. The

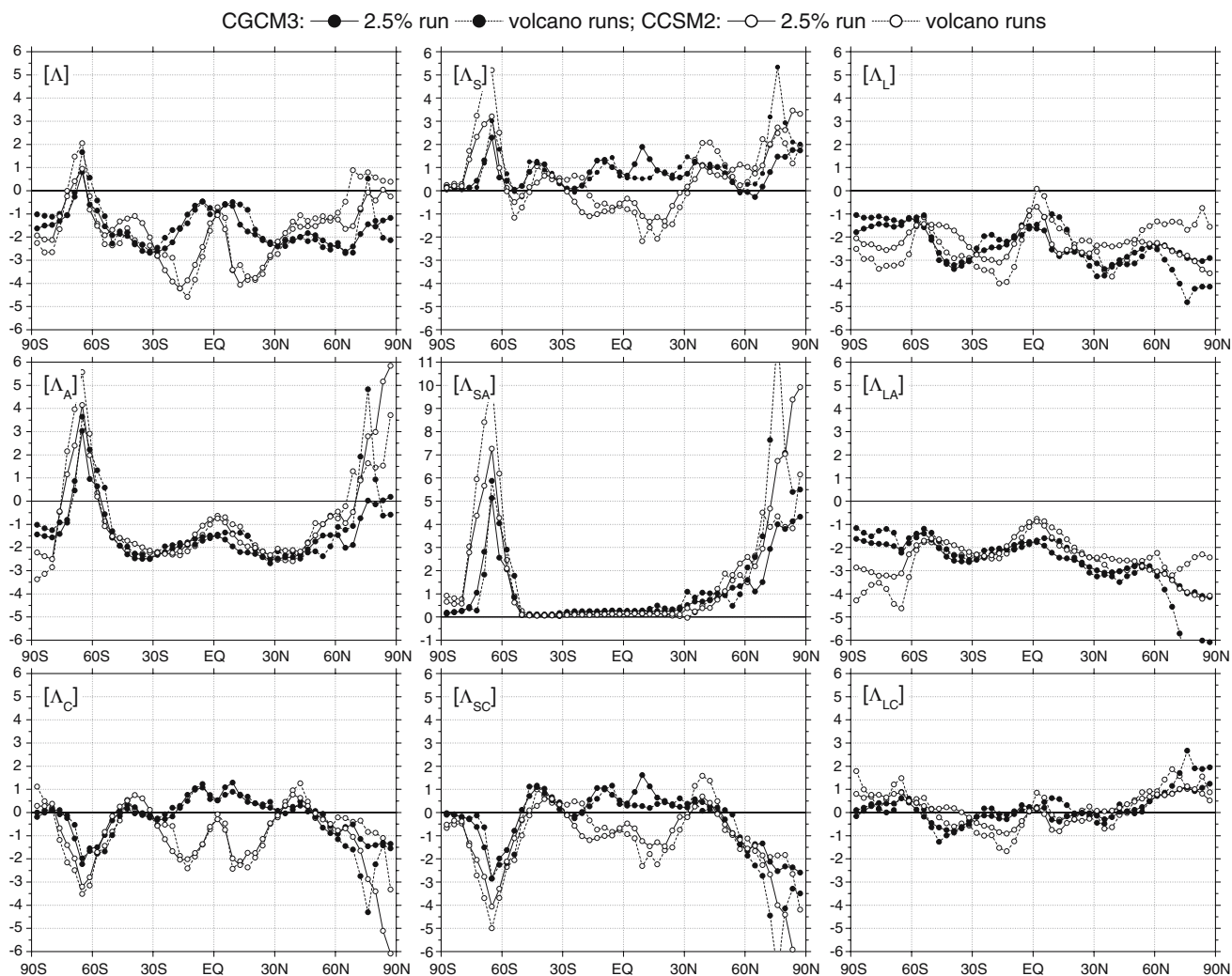


Fig. 11 The meridional structures of the feedback parameter and its components $[\Lambda] = [\Lambda_L] + [\Lambda_S] = [\Lambda_A] + [\Lambda_C] = [\Lambda_{LA}] + [\Lambda_{LC}] + [\Lambda_{SA}] + [\Lambda_{SC}]$ for the 2.5% solar constant increase case (average of years 41–50) and for the ensemble mean volcano-like forcing case (cumulative estimate to year 8). Units: $\text{Wm}^{-2} \text{K}^{-1}$

radiative forcing used corresponds to a comparatively large volcanic event and is imposed in an unambiguous way by varying the solar constant in the models. Three independent short-term volcano-like forcing experiments are performed with each model as well as longer-term simulations with constant forcing.

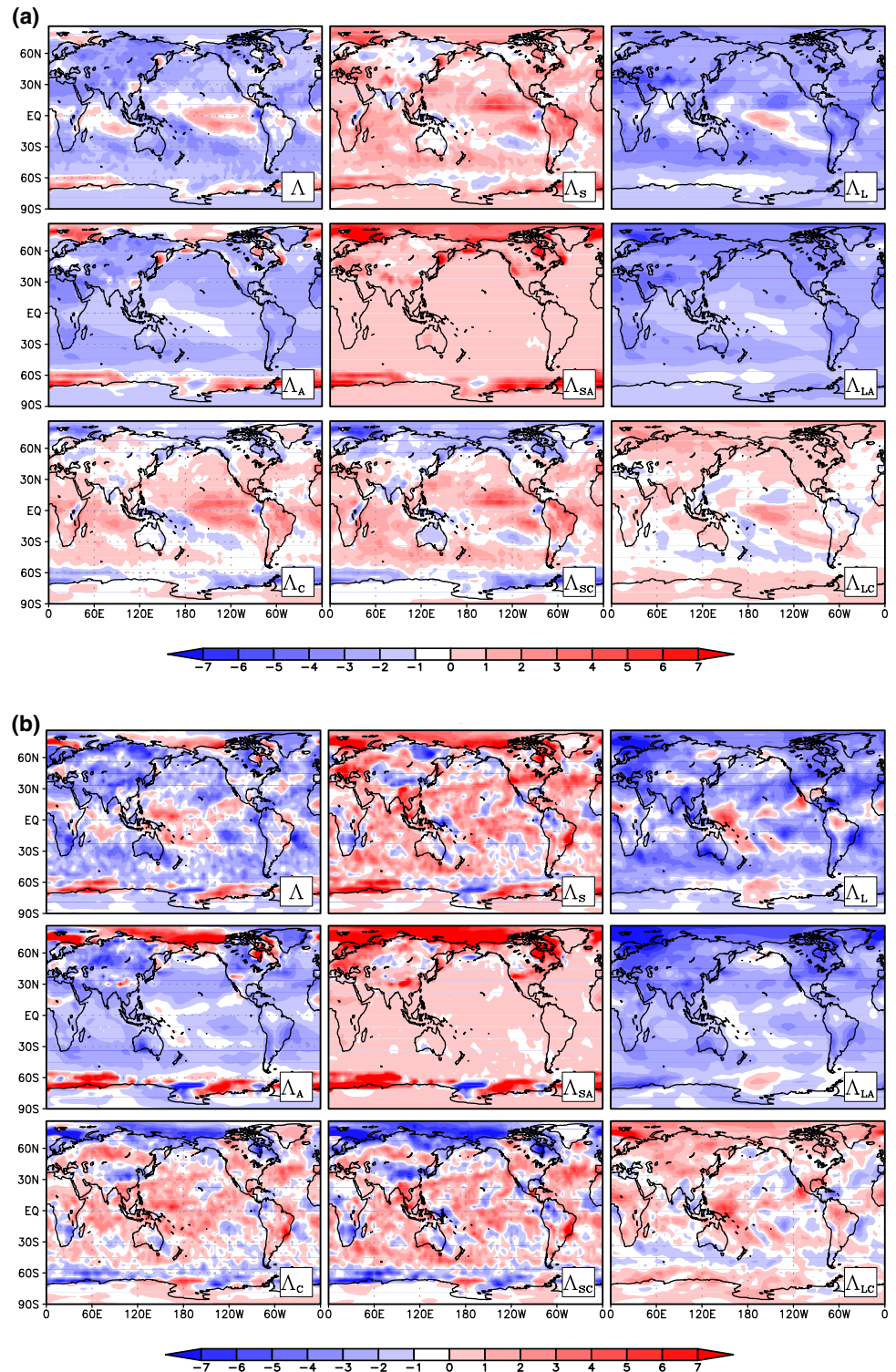
The global average temperature responses of the two models to the same volcano-like forcing are remarkably similar, despite the models' differing climate sensitivities. This immediately suggests that it is not possible to infer the climate sensitivity from the temperature response alone, even if the forcing of the system is known. In the modelled climate system at least, the change in the energy stored in the system, dominated by storage in the oceans, cannot be neglected. Inferring climate sensitivity by fitting to the

temperature curve directly produces an underestimate of the climate sensitivity of the modelled system.

If both the forcing and the heat storage of the system are known it is possible to obtain an estimate of the climate sensitivity and to distinguish between the differing climate sensitivities of the two models. The resulting estimate of climate sensitivity is larger than the equilibrium sensitivity on the order of 10–20%. For an individual volcanic event, the natural variability of the system constrains the accuracy of the estimate and the length and nature of the averaging of the data will affect the result. The accuracy of the inferred climate sensitivity also depends on the accuracy with which the temperature perturbation and the combined forcing and heat storage term are known. These accuracy requirements are seen to be daunting in general and, in

Fig. 12 The geographical patterns of the feedback and its components

$\Lambda = \Lambda_L + \Lambda_S = \Lambda_A + \Lambda_C = \Lambda_{LA} + \Lambda_{LC} + \Lambda_{SA} + \Lambda_{SC}$ for CGCM3. The *upper panels* give the results for the 2.5% solar constant increase case (average of years 41–50) and the *lower panels* the result for the ensemble mean volcano-like forcing case (cumulative estimate to year 8). Units: $\text{W m}^{-2} \text{K}^{-1}$

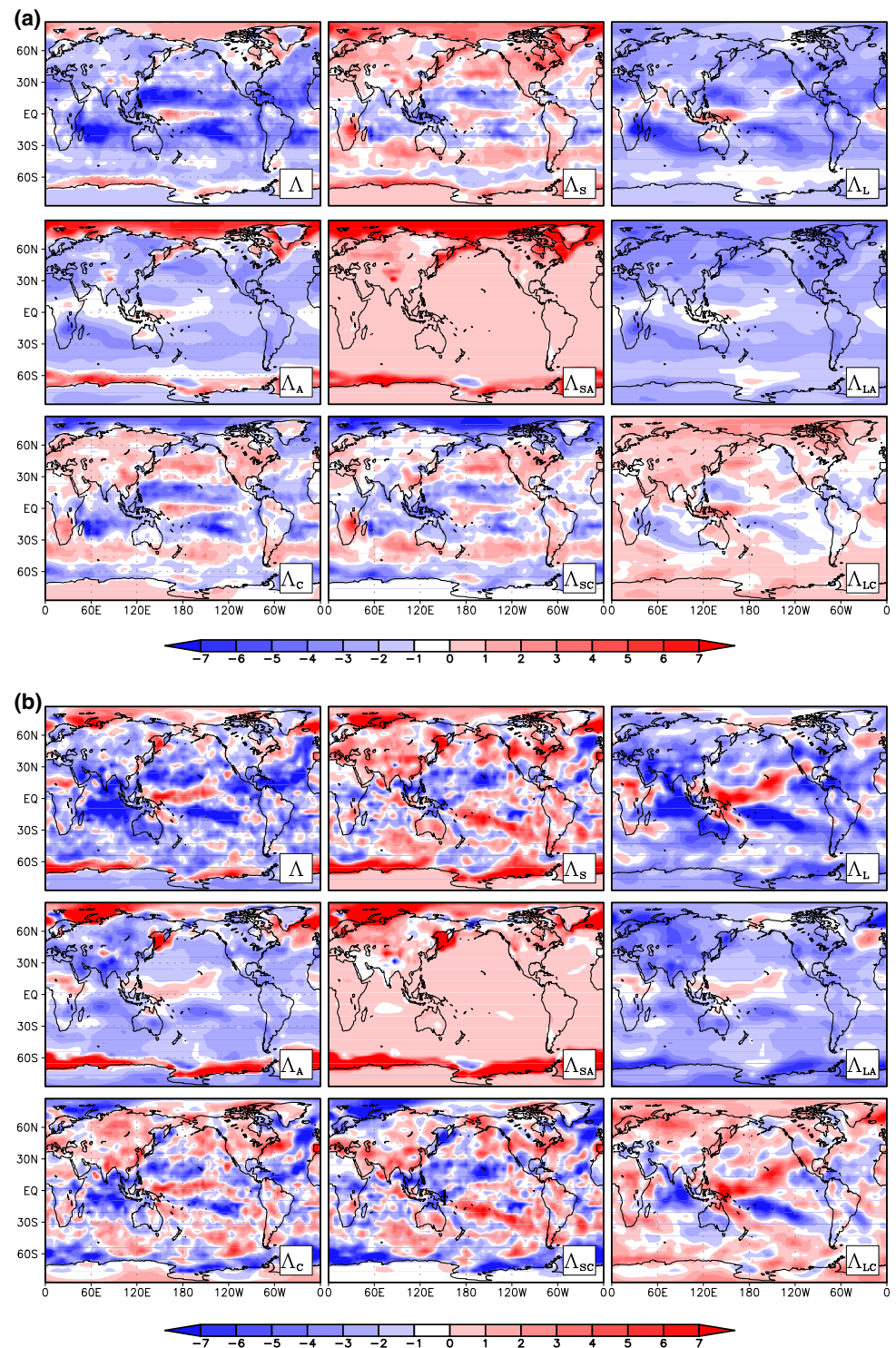


an actual case, knowledge of the forcing and heat storage would be problematic.

The decomposition of the geographical pattern of feedback into its several components indicates that the

climate feedback mechanisms operating in response to short-term volcano-like forcing are basically those operating also in longer-term constant forcing situations. The geographic patterns of the feedback

Fig. 13 As for Fig. 12 but for CCSM2



components in the two situations are qualitatively similar, particularly the more highly averaged north-south structures.

The basic conclusion is that it is possible to obtain an estimate of the equilibrium climate sensitivity of the

system from observations of strong volcanic events to within about 10% of the equilibrium value but that this requires that the forcing, the change in heat storage in the ocean and the temperature response all be known to high accuracy.

Acknowledgments Special thanks to Daniel Robatille for running the volcano-like simulations with the CCCma model and to K. von Salzen, G. Flato and F. Zwiers for comments on an earlier version. This research was supported in part by the Japan Agency for Marine-Earth Science and Technology (JAMSTEC) through its sponsorship of the International Pacific Research Center.

References

- Ammann C, Meehl G, Washington W, Zender C (2003) A monthly and latitudinally varying volcanic forcing data set in simulations of 20th century climate. *Geophys Res Lett* 30:1657–1660
- Barnett T, Pierce D, Schnur R (2001) Detection of anthropogenic climate change in the world's oceans. *Science* 292:270–274
- Boer GJ, Yu B (2003a) Climate sensitivity and response. *Clim Dyn* 20:415–429
- Boer GJ, Yu B (2003b) Climate sensitivity and climate state. *Clim Dyn* 21:167–176
- Boer GJ, Flato G, Ramsden D (2000) A transient climate change simulation with greenhouse gas and aerosol forcing: projected climate for the 21st century. *Clim Dyn* 16:427–450
- Boer GJ, Hamilton K, Zhu W (2005) Climate sensitivity and climate change under strong forcing. *Clim Dyn* 24:685–700
- Church JA, White NJ, Arblaster JM (2005) Significant decadal-scale impact of volcanic eruptions on sea level and ocean heat content. *Nature* 438:74–77
- Collins, WD, Ramaswamy D, Schwarzkopf MD, Sun Y, Portmann RW, Fu Q, Casanova SEB, Dufresne J-L, Fillmore DW, Forster PMD, Galin VY, Gohar LK, Ingram WJ, Kratz DP, Lefebvre M-P, Li J, Marquet P, Oinas V, Tsushima Y, Uchiyama T, Zhong WY (2006) Radiative forcing by well-mixed greenhouse gases: estimates from climate models in the IPCC AR4. *J Geophys Res* (in press)
- Douglass DH, Knox RS (2005a) Climate forcing by the volcanic eruption of Mount Pinatubo. *Geophys Res Lett* 32:L05710
- Douglass DH, Knox RS (2005b) Reply to comment by A. Robock on “Climate forcing by the volcanic eruption of Mount Pinatubo”. *Geophys Res Lett* 32:L20712
- Douglass DH, Knox RS (2005c) Reply to comment by T.M.L. Wigley et al. on “Climate forcing by the volcanic eruption of Mount Pinatubo”. *Geophys Res Lett* 32:L20710
- Flato GM, Boer GJ (2001) Warming asymmetry in climate change simulations. *Geophys Res Lett* 28:195–198
- Gregory J, Banks H, Stott P, Lowe J, Palmer M (2004) Simulated and observed decadal variability in ocean heat content. *Geophys Res Lett* 31:L15312
- Hansen J, Lacis A, Ruedy R, Sato M (1992) Potential climate impact of Mount Pinatubo eruption. *Geophys Res Lett* 19:215–218
- Hansen J, Sato M, Nazarenko L, Ruedy R, Lacis A, Koch D, Tegen I, Hall T, Shindell D, Santer B, Stone P, Novakov P, Thomason L, Wang R, Wang Y, Jacob D, Hollandsworth S, Bishop L, Logan J, Thompson A, Stolarski R, Lean J, Wilson R, Levitus S, Antonov J, Rayner N, Parker D, Christy J (2002) Climate forcings in Goddard Institute for Space Studies SI2000 simulations. *J Geophys Res* 107: DOI 10.1029/2001JD001143
- IPCC2001 (2001) Climate change 2001: the scientific basis. Third assessment report of the intergovernmental panel on climate change. Cambridge University Press, Cambridge, 881 pp
- IPCC2004 (2004) Workshop on climate sensitivity. intergovernmental panel on climate change. IPCC Working Group I Technical Support Unit, Boulder, 186 pp
- Ishii M, Kimono M, Kachi M (2003) Historical ocean subsurface temperature analysis with error estimates. *Mon Weather Rev* 131:51–73
- Kiehl J, Gent P (2004) The community climate system model, version 2. *J Clim* 17:3666–3682
- Levitus S, Antonov J, Wang J, Delworth T, Dixon K, Broccoli A (2001) Anthropogenic warming of the Earth's climate system. *Science* 292:267–270
- Levitus S, Antonov J, Boyer T (2005) Warming of the World Ocean, 1955–2003. *Geophys Res Lett* 32:L02604
- Press W, Flannery B, Teukolsky S, Vetterling W (1992) Numerical recipes in Fortran; the art of scientific computing. Cambridge University Press, Cambridge
- Raper S, Gregory J, Stouffer R (2002) The role of climate sensitivity and ocean heat uptake on AOGCM transient temperature response. *J Clim* 15:124–130
- Robock A (2000) Volcanic eruptions and climate. *Rev Geophys* 38:191–219
- Robock A (2005) Comment on “Climate forcing by the volcanic eruption of Mount Pinatubo” by David H Douglass and Robert S Knox. *Geophys Res Lett* 32:L20711
- Robock A, Mao J (1995) The volcanic signal in surface temperature observations. *J Clim* 8:1086–1103
- Scinocca JF, McFarlane NA (2004) The variability of modeled tropical precipitation. *J Atmos Sci* 61:1993–2015
- Senior CA, Mitchell J (2000) The time-dependence of climate sensitivity. *Geophys Res Lett* 27:2685–2689
- Stenchikov G, Robock A, Ramaswamy V, Schwarzkopf MD, Hamilton K, Ramachandran S (2002) Arctic oscillation response to the 1991 Mount Pinatubo eruption: effects of volcanic aerosols and ozone depletion. *J Geophys Res* 107:4803–4818
- Stenchikov G, Hamilton K, Stouffer R, Robock A, Ramaswamy V, Santer B, Graf H-F (2006) Arctic oscillation response to volcanic eruptions in the IPCC AR4 climate models. *J Geophys Res* 111. DOI 10.1029/2005JD006286
- Stowasser M, Hamilton K, Boer GJ (2006) Local and global climate feedbacks in models with differing climate sensitivities. *J Clim* 19:193–209
- Sun S, Hansen J (2003) Climate simulations for 1951–2050 with a coupled atmosphere–ocean model. *J Clim* 16:2807–2826
- Wigley T, Ammann C, Santer B, Taylor K (2005a) Comment on “Climate forcing by the volcanic eruption of Mount Pinatubo” by David H. Douglass and Robert S. Knox. *Geophys Res Lett* 32:L20709
- Wigley T, Ammann C, Santer B, Raper S (2005b) Effect of climate sensitivity on the response to volcanic forcing. *J Geophys Res* 110:D09107
- Yokohata T, Emori S, Nozawa N, Tsushima Y, Ogura T, Kimoto M (2005) Climate response to volcanic forcing: validation of climate sensitivity of a coupled atmosphere–ocean general circulation model. *Geophys Res Lett* 32:L21710
- Zhang J, Christopher SA, Remer LA, Kaufman YJ (2005) Shortwave aerosol radiative forcing over cloud-free oceans from Terra: 2. Seasonal and global distributions. *J Geophys Res* 110. DOI 10.1029/2004JD005009